Epilepsy Research 150 (2019) 78–94

Contents lists available at ScienceDirect

Epilepsy Research

journal homepage: www.elsevier.com/locate/epilepsyres

Sustained somatostatin gene expression reverses kindling-induced increases in the number of dividing Type-1 neural stem cells in the hippocampi of behaviorally responsive rats

Jeffrey A. Leibowitz[a], Gowri Natarajan[d,e], Junli Zhou[d,e], Paul R. Carney[d,e,f], Brandi K. Ormerod[a,b,c,*]

[a] J. Crayton Pruitt Family Department of Biomedical Engineering, USA
[b] Department of Neuroscience, USA
[c] McKnight Brain Institute, USA
[d] Department of Neurology and Pediatrics, USA
[e] Neuroscience Program, USA
[f] Carolina Institute for Developmental Disabilities, University of North Carolina at Chapel Hill, Chapel Hill, NC, 27599, USA

ARTICLE INFO

Keywords:
Temporal lobe epilepsy
Adult neurogenesis
Neural stem cells (NSCs)
Neural progenitor cells (NPCs)
Type-1 NSCs
Type-2 NPCs
Hippocampus
Somatostatin (SST)
Kindling
Adeno-associated viral (AAV) vectors
Gene therapy

ABSTRACT

Neurogenesis persists throughout life in the hippocampi of all mammals, including humans. In the healthy hippocampus, relatively quiescent Type-1 neural stem cells (NSCs) can give rise to more proliferative Type-2a neural progenitor cells (NPCs), which generate neuronal-committed Type-2b NPCs that mature into Type-3 neuroblasts. Many Type-3 neuroblasts survive and mature into functionally integrated granule neurons over several weeks. In kindling models of epilepsy, neurogenesis is drastically upregulated and many new neurons form aberrant connections that could support epileptogenesis and/or seizures. We have shown that sustained vector-mediated hippocampal somatostatin (SST) expression can both block epileptogenesis and reverse seizure susceptibility in fully kindled rats. Here we test whether adeno-associated virus (AAV) vector-mediated sustained SST expression modulates hippocampal neurogenesis and microglial activation in fully kindled rats. We found significantly more dividing Type-1 NSCs and a corresponding increased number of surviving new neurons in the hippocampi of kindled versus sham-kindled rats. Increased numbers of activated microglia were found in the granule cell layer and hilus of kindled rats at both time points. After intrahippocampal injection with either eGFP or SST-eGFP vector, we found similar numbers of dividing Type-1 NSCs and -2 NPCs and surviving $BrdU^+$ neurons and glia in the hippocampi of kindled rats. Upon observed variability in responses to SST-eGFP (2/4 rats exhibited Grade 0 seizures in the test session), we conducted an additional experiment. We found significantly fewer dividing Type-1 NSCs in the hippocampi of SST-eGFP vector-treated responder rats (5/13 rats) relative to SST-eGFP vector-treated non-responders and eGFP vector-treated controls that exhibited high-grade seizures on the test session. The number of activated microglia was upregulated in the GCL and hilus of kindled rats, regardless of vector treatment. These data support the hypothesis that sustained SST expression exerts antiepileptic effects potentially through normalization of neurogenesis and suggests that abnormally high proliferating Type-1 NSC numbers may be a cellular mechanism of epilepsy.

1. Introduction

Thousands of granule neurons are added daily throughout life to the hippocampal dentate gyrus (Altman, 1962; Cameron et al., 1993; Eriksson et al., 1998). Neurogenesis in the healthy adult mammalian hippocampus consists of several steps that can begin with the proliferation of relatively quiescent Type-1 cells, considered to be the neural stem cells (NSCs) of the hippocampus (Aimone et al., 2014; Kronenberg et al., 2003; Seri et al., 2001). More regularly, adult hippocampal neurogenesis is thought to begin with the proliferation of uncommitted Type-2a neural progenitor cells (NPCs), which can give rise to neuron-committed Type-2b NPCs that differentiate into Type-3

* Corresponding author at: J. Crayton Pruitt Family Department of Biomedical Engineering, Herbert Wertheim College of Engineering, University of Florida, 1275 Center Drive, JG296, Gainesville, FL, 32611-0296, USA.
E-mail address: bormerod@bme.ufl.edu (B.K. Ormerod).

https://doi.org/10.1016/j.eplepsyres.2019.01.005
Received 5 November 2018; Received in revised form 18 December 2018; Accepted 10 January 2019
Available online 11 January 2019
0920-1211/

neuroblasts. About one half of these neuroblasts survive and mature into functional neurons over several weeks (Cameron and McKay, 2001; Filippov et al., 2003; Kempermann et al., 2004; Seri et al., 2001; van Praag et al., 2002). Exposure to stimuli like physical activity, social and environmental enrichment, alcohol or withdrawal from alcohol can each increase neurogenesis by variably stimulating Type-2a NPC, Type-2b NPC or occasionally Type-3 neuroblast proliferation or by promoting new neuron survival (Kronenberg et al., 2003; Nickell et al., 2017; Olson et al., 2006; van Praag et al., 1999b). Understanding how physiologic stimuli may affect neurogenesis through unique neural stem and progenitor cell populations may reveal mechanisms underlying phenotypic outcomes and provide novel therapeutic targets for disease. The increased number of new neurons stimulated by physical activity or enrichment in aging models or in young animals housed in standard colony conditions is associated with better scores in hippocampus-dependent cognitive tasks, therefore, targeting NPC populations affected by these stimuli may alleviate associated comorbidities (Gonçalves et al., 2016; Speisman et al., 2013a, b; van Praag et al., 2005). Whether the supraphysiological stimulation of division among these NPC populations or the stimulation of the relatively quiescent NSC population leads to aberrant neurogenesis or impaired function is currently unclear.

A wide range of epilepsy models has demonstrated that chemical and electrical kindling leads to a supraphysiological increase in hippocampal neurogenesis (Nakagawa et al., 2000; Parent et al., 2006, 1998). Newborn neurons produced in the kindled brain often exhibit ectopic migration, aberrant mossy fiber sprouting and abnormal hilar basal dendrites (Fournier et al., 2010, 2013; Jessberger et al., 2007b; Kron et al., 2010; Parent et al., 2006, 1998; Pekcec and Potschka, 2007). The exaggerated production of new neurons with aberrant connectivity has been hypothesized to contribute to epileptogenesis, seizure maintenance and the cognitive impairments exhibited by individuals with epilepsy (Botterill et al., 2015; Cho et al., 2015; Fournier et al., 2013; Jessberger and Parent, 2015; Scharfman and Hen, 2007). Indeed, ablating neurogenesis can reduce the frequency of spontaneous seizures and the occurrence of aberrant seizure-induced plasticity after chemical kindling (Cho et al., 2015; Jung et al., 2004, 2006; Kron et al., 2010) and driving ectopic or exaggerated neurogenesis can produce seizures (Pun et al., 2012; Scharfman et al., 2005, 2002). Additionally, anti-epileptic drugs can block the neurogenic effects of kainic acid and protect rats from seizure-induced cognitive impairment (Jessberger et al., 2007a). Interestingly, targeted gamma irradiation, anti-mitotic agents and genetic ablation strategies that drastically reduce neurogenesis also reduce the number and duration of seizures (Cho et al., 2015; Hüttmann et al., 2003; Jung et al., 2004; Monje et al., 2002; Parent et al., 1999; Pekcec et al., 2008; Steiner et al., 2008). These data suggest that aberrant neurogenesis could support the development and maintenance of seizures in temporal lobe epilepsy and in animal models of temporal lobe epilepsy.

We have shown that sustained adeno-associated viral (AAV) vector-mediated somatostatin (SST) expression can block epileptogenesis in adult rats and prevent seizures in a subgroup of rats already amygdala-kindled to a seizure-susceptible state (Natarajan et al., 2017; Zafar et al., 2012). SST is a neuropeptide that, along with its 5 G-protein-coupled receptors, is expressed in the naïve rodent hippocampus predominantly in the CA1 region, CA3 region and on hilar GABAergic neurons (Freund and Buzsáki, 1996; Schindler et al., 1996, 1997; Schulz et al., 2000). Our observed anti-epileptic effect is consistent with the observations that inhibitory SST-expressing hilar neurons are selectively vulnerable to death in individuals with epilepsy and in animal temporal lobe epilepsy models, that reduced SST levels increase kindling rates and seizure severity, and that SST receptor agonists have anticonvulsant effects (Aourz et al., 2011; Bezchlibnyk et al., 2007; Buckmaster and Dudek, 1997; Buckmaster et al., 2002; Monno et al., 1993; Robbins et al., 1991; Sloviter, 1987; Vezzani et al., 1991). In addition, SST delivery to CA1 and CA3 regions inhibits epileptiform activity by blocking presynaptic glutamate release and by modulating postsynaptic voltage-sensitive potassium channels and lateral performant path long-term potentiation (Baratta et al., 2002; Kapur, 2013; Olias et al., 2004; Qiu et al., 2008; Schindler et al., 1996; Tallent and Siggins, 1997). We hypothesized that since SST is anti-proliferative in other tissues (Leu et al., 2008; Nolan et al., 2007), sustained SST expression may also normalize kindling-induced changes in adult hippocampal neurogenesis. We expected that if kindling-induced seizures were related to upregulated and perhaps aberrant neurogenesis, then normalizing neurogenesis with sustained vector-mediated SST gene expression may reduce seizure severity in rats kindled to a seizure-susceptible state.

In *Experiment 1*, we tested the effects of amygdala kindling on the number and phenotype of dividing NSCs/NPCs and their progeny. In *Experiment 2*, we tested whether sustained vector-mediated SST expression impacted the number and phenotype of NSCs/NPCs and their progeny in the hippocampi of kindled rats. In *Experiment 3*, we tested whether sustained SST expression differentially impacted the effects of kindling on neurogenesis in responder and non-responder rats. Since adult neurogenesis is sensitive to neuroinflammation (Ekdahl et al., 2003; Monje et al., 2003; Ormerod et al., 2013) and kindling stimulates a neuroinflammatory response (Khurgel and Ivy, 1996; Plata-Salamán et al., 2000), we quantified the effects of kindling on resting and activated microglia numbers and the strength of their relationship with dividing NSC and NPC numbers or surviving new neuron numbers in each experiment.

2. Materials and methods

2.1. Subjects

All rats used in this study were treated in accordance with Federal and University of Florida Institutional Animal Care and Use Committee regulations regarding the ethical use of animals for experimentation. Adult male Sprague Dawley rats (n = 45 250–275 g; Envigo) were housed in pairs upon arrival in corn-cob lined ventilated shoebox cages located in a standard colony room maintained on a 12:12 h light:dark cycle (lights on at 6:00AM) at 24 ± 1 °C. Following surgical implantation of electrodes, rats were housed individually to minimize the likelihood of head-stage losses. In either case, they were given free access to Harlan Teklad Rodent Food Diet #7912 and reverse osmosis-filtered water for the duration of each experiment.

Fig. 1 illustrates the methods used in *Experiments 1–3*. In all experiments, rats underwent amygdala kindling in twice daily sessions (≥6 h apart) until they exhibited a Grade 5 seizure in 3 consecutive sessions. *Experiment 1* tested the effects of kindling on the number of dividing $BrdU^+$ Type-1 NSCs and Type-2 NPCs and on the number and phenotype of surviving $BrdU^+$ new cells. Sham-kindled rats (no electrical stimulation was administered) and kindled rats were injected with BrdU 48 h after a kindled rat achieved criterion. Rats were perfused 4 h later to quantify and phenotype dividing $BrdU^+$ cells or 4 weeks later to quantify and phenotype surviving $BrdU^+$ cells (n = 5 rats per group). *Experiment 2* tested the effects of sustained SST expression on the number of dividing EdU^+ Type-1 NSCs and Type-2 NPCs and on the number and phenotype of $BrdU^+$ surviving new cells in kindled rats. Rats were injected with BrdU 48 h after achieving criterion and then eGFP or SST-eGFP (n = 4 rats per group) vector was infused bilaterally into their hippocampi the following week. After a 3-week recovery, the rats were given a test session, post-test sessions every 48 h for ~2.5 weeks, injected with EdU 48 h after the final post-test session and then perfused 4 h later to quantify the number and phenotype of dividing EdU^+ cells and of surviving $BrdU^+$ cells. *Experiment 3* tested whether kindling differentially affected the number of dividing $BrdU^+$ Type-1 NSCs or Type-2 NPCs in eGFP vector-treated (n = 4), SST-responder rats that exhibited Grade 0 seizures on the test stimulation (n = 5) and SST-non-responders that exhibited seizures ≥

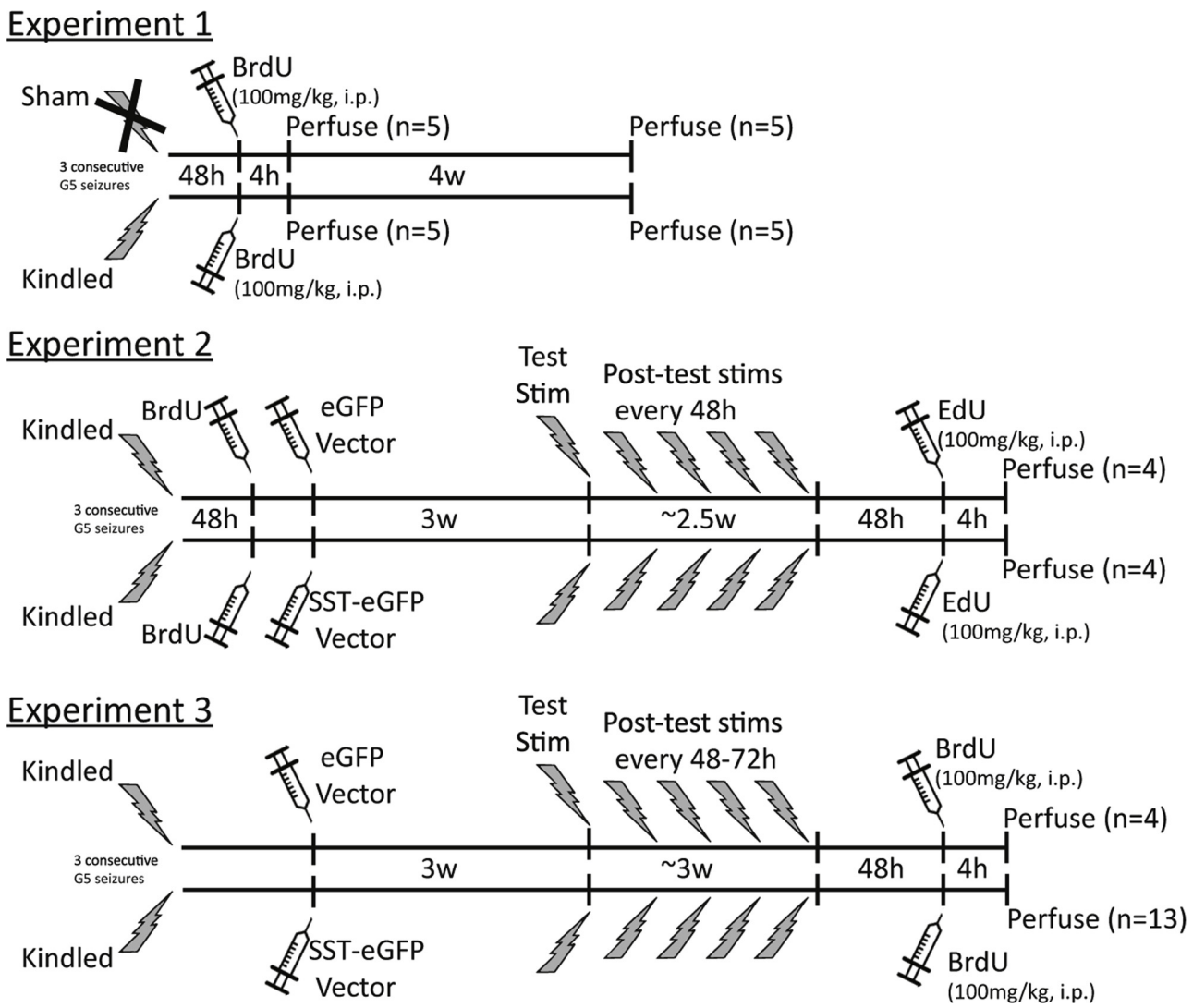

Fig. 1. Schematic of experiment designs. *Experiment 1* tested the effects of kindling on the number of dividing Type-1 neural stem cells and Type-2 neural progenitor cells and the survival of their progeny. Rats were kindled to criterion or sham-kindled and then injected with BrdU (100 mg/kg) 48 h later. Kindled and sham-kindled rats were perfused 4 h later to quantify the number and phenotype of dividing cells or 4 weeks later (n = 5 per group) to quantify the number and phenotype of their progeny. *Experiment 2* tested the effects of sustained SST gene expression on the number and phenotype of surviving cells 6 weeks after kindling and on the number of dividing Type-1 NSCs and Type-2 NPCs. Rats were kindled to criterion and then injected with BrdU (100 mg/kg) 48 h later and then injected intrahippocampally with either eGFP or SST-eGFP vector. They received one test stimulation 3 weeks later followed by periodic post-test stimulations for an additional 3 weeks to test persistence of kindling and vector effects. eGFP- and SST-eGFP vector-treated rats were injected with EdU (100 mg/kg) 48 h after their last post-test stimulation and perfused 4 h later (n = 4 and n = 4, respectively) to quantify surviving and dividing cells. *Experiment 3* tested the effects of sustained SST gene expression on the number of dividing Type-1 NSCs and Type-2 NPCs. Rats were kindled until criterion and then injected intrahippocampally with either eGFP or SST-eGFP vector. They received one test stimulation 3 weeks later followed by periodic post-test stimulations for an additional 3 weeks to test persistence of kindling and vector effects. eGFP- and SST-eGFP vector-treated rats were injected with BrdU (100 mg/kg) 48 h after their last post-test session and perfused 4 h later (n = 4 and n = 13, respectively) to quantify the number and phenotype of dividing cells.

Grade 1 on the test stimulation (n = 8) rats. eGFP vector or SST-eGFP vector was infused into the hippocampi of rats the week after they achieved criterion. After a 3-week recovery, the rats were given a test session, post-test sessions every 48–72 h over ˜3 weeks, injected with BrdU 48 h after the final post-test session and then perfused 4 h later to quantify and phenotype dividing $BrdU^+$ cells. Relationships between numbers of microglia and numbers of dividing NSCs, dividing NPCs and new neurons were tested in each experiment.

2.2. Electrode implantation

Two weeks after arrival, rats were implanted with bipolar local electrical field potential recording and stimulating electrodes (330 µm d; impedance confirmed as < 1.8 Ω) that were made in-house, as detailed previously (Natarajan et al., 2017; Zafar et al., 2012). Briefly, anesthetized rats were placed in a Kopf stereotaxic frame so that a bipolar electrode could be implanted into each amygdala (−2.2 mm AP, ± 4.8 mm ML, −8.3 mm DV) according to Paxinos and Watson (Paxinos and Watson, 2007) to record and stimulate activity in the left and right hemispheres of the rats, counterbalanced within and between groups. In *Experiments 2 and 3*, small plastic hex nuts with removable screws were placed over dentate gyrus and CA1 region target coordinates to keep the skull free of dental cement so that vector could be delivered at a later time point. Ground and reference electrodes were implanted rostral to bregma and caudal to lambda, respectively. All electrodes were then attached to male Amphenol pins that were inserted into plastic connector strips that were 3D-printed at the University of Florida Infinity Fabrication laboratory (http://fablab.arts.ufl.

edu/). The entire assembly was secured with dental cement to bone screws anchored to the skull.

2.3. Electrical kindling

Synchronized behavioral and electroencephalographic (EEG) data were recorded in all kindling, test and post-test sessions to grade behavioral seizures and to confirm the presence or absence of afterdischarges (ADs) or epileptiform bursts (Racine et al., 1972). After a 10 d recovery from surgery, rats were tested in a baseline session to identify the AD threshold current that would be employed in all subsequent kindling, test and post-test sessions. A standard 2 s, 1 ms pulse duration, 50 Hz biphasic square wave pulse was delivered at 1 min inter-stimulus intervals (initially at 50 μA but stepped up 50 μA in intensity every delivery) until an AD was observed in the EEG (Natarajan et al., 2017; Racine, 1972; Zafar et al., 2012). An AD was defined as spikes > 1 Hz with amplitudes greater than twice the spike amplitudes detected in the baseline EEG (Natarajan et al., 2017; Zafar et al., 2012). Sham-kindled rats were treated similarly to kindled rats but did not receive electrical current.

Beginning 24 h later, the AD threshold current identified for each rat was delivered in kindling sessions administered twice daily (≥6 h apart) until that rat exhibited a Grade 5 seizure in 3 consecutive sessions. Seizures were graded according to the Racine scale of seizure severity in animal epilepsy models (Racine, 1972), in which Grade 0 reflects no behavioral change; Grade 1 reflects staring, immobility, and facial movements; Grade 2 reflects head nodding and chewing; Grade 3 reflects unilateral forelimb clonus; Grade 4 reflects bilateral forelimb clonus with rearing; Grade 5 reflects bilateral forelimb clonus with rearing, loss of balance, and falling. In *Experiments 2* and *3*, a single test session was administered 3 weeks after vector injection to quantify the effect of vector treatment on seizure grade, followed by post-test sessions to quantify the resilience of the effects (see Fig. 1 and the subjects section for details).

The synchronized behavioral and EEG data collected during kindling sessions were scored to quantify: 1) AD threshold currents (μA); 2) number of sessions to exhibit the first Grade 5 seizure; 3) number of high-grade (Grade 4–5) seizures; and 4) sessions to criterion (the number of sessions required to exhibit a Grade 5 seizure over 3 consecutive sessions). Seizure grades were scored and the presence or absence of ADs were confirmed in EEGs on test and post-test sessions.

2.4. BrdU and EdU preparation and injections

Bromodeoxyuridine (BrdU; Sigma Aldrich, St. Louis, MO) and ethynyldeoxyuridine (EdU; Life Technologies, Eugene, OR) were dissolved in freshly prepared sterile isotonic saline at a concentration of 20 mg/ml and 10 mg/ml, respectively. BrdU (100 mg/kg) was injected intraperitoneally (i.p.) 48 h after rats reached criterion in *Experiments 1* and *2* or 48 h after the final post-test session in *Experiment 3*. EdU (100 mg/kg) was injected i.p. 48 h after the final post-test session in *Experiment 2*. This dose of BrdU and EdU was employed because it effectively labels dividing hippocampal NSCs and NPCs when single injections are employed (Burns and Kuan, 2005; Cameron and McKay, 2001; Zeng et al., 2010).

2.5. AAV vector construct and injections

We detailed construction of the AAV5-CBa-preproSST-eGFP (the 'SST-eGFP vector') and the AAV5-CBa-eGFP (the 'eGFP vector') vector previously (Natarajan et al., 2017). The plasmid sequence included the hybrid cytomegalovirus enhancer/chicken β-actin (CBa) promoter driving the expression of either a preproSST transgene plus a downstream eGFP reporter, or an eGFP reporter alone. An internal ribosomal entry site sequence was inserted between preproSST and eGFP coding sequences of the SST-eGFP vector so that eGFP expression reported preproSST expression. Briefly, the CBa-eGFP plasmid was packaged into serotype 5 AAV capsids in one batch for both Experiments 2 and 3 (gtc.ufl.edu/core/vector-core-lab.htm; titer = 8.9×10^{12} vg/ml) and the CBa-SST-eGFP plasmid was packaged into serotype 5 AAV capsids in one batch for *Experiment 2* (SAB tech Inc., Philadelphia, PA; titer = 1.0×10^{13} vg/ml) and in 2 batches for *Experiment 3* (gtc.ufl.edu/core/vector-core-lab.htm; titer = 6.1×10^{12} vg/ml or 4.9×10^{13} vg/ml). In *Experiment 3*, SST-eGFP vector-treated rats were grouped because we found no statistically significant effects of SST-eGFP vector titer on test session seizure grade, post-test session seizure grade or on histological variables associated with neuroinflammation or neurogenesis.

In the rat hippocampus, preproSST yields proSST that is cleaved into neuronostatin-13 by a yet to be identified peptidase and into either SST-14 by prohormone convertase 1 (PC1) and PC2 or the N-terminal expanded isoform SST-28 by furin-like peptidases, such as carboxypeptidase-E (CPE) and furin (Billova et al., 2007; Samson et al., 2008). Pan SST antibodies reveal strong SST expression in hippocampal principal neurons and interneurons, high-level CPE and PC2 expression and low to moderate PC1 expression (Billova et al., 2007; Viollet et al., 2008). While SST-14 is the predominant natural CNS SST isoform, both SST-14 and SST-28 are expressed in the brain and bind with similar affinities to the four G protein-coupled SST receptors (SSTRs) expressed in the hippocampus (Csaba and Dournaud, 2001; Dun et al., 2010; Olias et al., 2004; Reisine and Bell, 1995; Viollet et al., 2008). In the hippocampus, neuronostatin-13/SST-14 protein concentration ratios and expression of the putative neuronostatin receptor GPR107 are extremely low and numbers of neuronostatin producing neurons are sparse (Dun et al., 2010; Samson et al., 2016, 2008). While the effects of the SST-eGFP vector could be produced by SST, neuronostatin or a combination of both peptides, these data suggest that the effects of the SST-eGFP vector are likely mediated through sustained SST expression.

In *Experiments 2* and *3*, eGFP or SST-eGFP vector was injected bilaterally into the dentate gyri and CA1 regions of rats in the week after they achieved criterion, as we described previously (Natarajan et al., 2017). Anesthetized rats were mounted in a Kopf stereotaxic frame and the placeholder screws were removed from the hex nuts that had been placed over injection target regions during the initial electrode placement surgery so that holes could be drilled. The eGFP or SST-eGFP vector was infused through a 10 μl Hamilton syringe fitted with a 27 G steel needle by an infusion system (Cole-Parmer, Vernon Hills, IL) into each dentate gyrus (−3.8 mm AP, ± 1.88 mm ML, −3.4 mm DV) and CA1 region (−3.8 mm AP, ± 1.88 mm ML, −2.4 mm DV) according to Paxinos and Watson (Paxinos and Watson, 2007) at a flow rate of 0.3 μl/min. A 2 μl volume was infused into each of the 4 injection sites.

2.6. Perfusion and histology

Four hours or 4 weeks after the final cell synthesis marker injection, rats were anesthetized with a xylazine (10 mg/kg) and ketamine (80 mg/kg) cocktail injected i.p. and then perfused with ice-cold isotonic saline followed by ice-cold, freshly prepared 4% paraformaldehyde (Electron Microscopy Sciences; Hatfield, PA) in phosphate-buffered saline (PBS). Brains were extracted, post-fixed overnight in perfusate at 4 °C and then cryoprotected in 30% sucrose solution for 2–3 d. The brains were then sectioned coronally at 40 μm through the rostral-caudal extent of the hippocampus on a freezing stage microtome (American Optical Corporation; Buffalo, NY). Brain sections were stored in cryoprotectant solution (25% glycerol, 30% ethylene glycol and 45% 0.1 M PBS) at −20 °C until processed immunohistochemically.

Electrode placements in the amygdalae of all rats were confirmed in histological sections. Fig. 2 shows a schematic of the hippocampus regions that the vector infusion targeted and a representative image of eGFP expression in the hippocampus of a kindled rat. An experimenter blind to the vector treatment group and seizure grades of the rats confirmed bilateral eGFP expression through at least 1 major hippocampal region (the CA1 region, CA3 region and/or dentate gyrus) in all

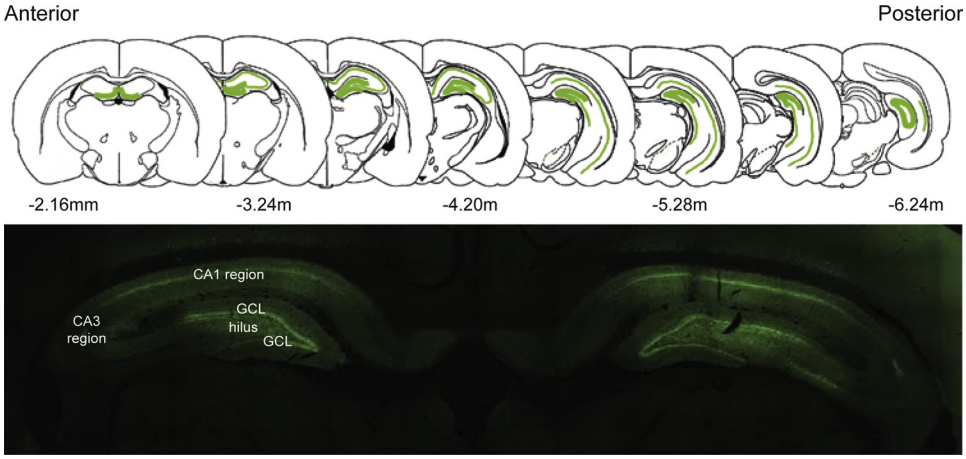

Fig. 2. Schematic showing vector target regions in the hippocampus and a confocal image of eGFP expression in a hippocampal section of a SST-eGFP vector-treated rat. Vector was injected bilaterally into the dentate gyrus and CA1 region (2 µl per injection site). Bilateral eGFP expression was detected through the rostral-caudal extent of at least 1 major hippocampal subfield (the CA1 region, CA3 region and/or dentate gyrus) of all rats and moderate to strong bilateral eGFP expression was found through the CA1 and CA3 region of most rats. eGFP expression was detected in the cortex dorsal to and thalamic regions ventral to the hippocampus of some rats. No overt differences in eGFP expression were found between eGFP vector-treated, SST-eGFP vector-treated responder and SST-eGFP vector-treated non-responder groups.

rats. Moderate to strong bilateral eGFP expression was found through the CA1 and CA3 region of most rats and eGFP expression was also noted in the cortex dorsal to and thalamic regions ventral to the hippocampus of some rats. No overt differences in eGFP expression were found between eGFP vector-treated, SST-eGFP vector-treated responder and non-responder groups.

2.7. Immunohistochemistry

Immunohistochemistry was performed on free-floating sections and the sections were rinsed with tris-buffered saline (TBS; pH 7.4) repeatedly between steps. Blocking solution and antibody diluent was 3% normal donkey serum and 0.1% Triton-X in TBS.

2.7.1. Enzyme substrate immunostaining and Click-IT chemistry

$BrdU^+$, EdU^+, and Iba-1^+ cells were revealed enzymatically on separate sets of sections so that total cell numbers could be estimated using stereological principles. To reveal $BrdU^+$ and Iba-1^+ cells, sections were incubated in 0.3% H_2O_2 for 10 min at room temperature (RT) to quench endogenous peroxidase and then in blocking solution for 20 min at RT. Sections being processed to reveal BrdU were next rinsed in 0.9% NaCl and then incubated in 2 N HCl for 20 min at 37 °C to denature DNA. Sections were then incubated overnight at 4 °C in rat anti-BrdU (1:500; AbD Serotec, Raleigh, NC) or rabbit anti-Iba-1 (1:1000; Wako Chemicals, Wako, TX) and then in biotinylated anti-rat IgG or anti-rabbit IgG (1:500; Jackson Immunoresearch, West Grove, PA), respectively for 4 h at RT. The sections were incubated in avidin-biotin horseradish peroxidase (Vector Labs, Burlingame, CA) for 2 h at RT and then reacted in a solution of 0.02% 3,3′-diaminobenzidine tetrahydrochloride (DAB; Sigma Aldrich, St. Louis, Mo) and 0.5% H_2O_2 for ~3 min. EdU^+ cells were revealed on sections processed using the Click-iT EdU Colorimetric IHC detection kit (Life Technologies, Eugene, OR) according to kit instructions using kit reagents. Briefly, sections were incubated in 0.3% H_2O_2 for 10 min at RT to quench endogenous peroxidase, Trypsin-EDTA buffer for 20 min at RT to permeabilize the tissue, freshly prepared Click-IT reaction cocktail for 1 h at RT, streptavidin-peroxidase reaction cocktail for 2 h at RT and then reacted in DAB reaction buffer for 3 min. All sections were mounted on Fisher Superfrost microscope slides, dried overnight, dehydrated under an ethanol series, cleared in xylene and then coverslipped under Permount (Thermo Fisher Scientific). Sections stained to reveal EdU^+ and Iba-1^+ cells were counterstained with 0.25% Cresyl Violet acetate (Sigma Aldrich) during dehydration to assist with cell counting.

2.7.2. Fluorophore immunostaining

The phenotypes of dividing $BrdU^+$ cells, surviving $BrdU^+$ cells, dividing EdU^+ cells, and Iba-1^+ microglia were each revealed on separate sets of 3–4 sections from a randomly selected 1 in 12 series for each rat using maximally cross-adsorbed fluorophore-conjugated secondary antibodies.

EdU^+ cells were first revealed using the Click-iT EdU Alexa Fluor 555 imaging kit (Life Technologies, Eugene, OR) according to kit instructions. Briefly, sections were reacted in freshly prepared Click-IT reaction cocktail for 1 h at RT and then fixed in 4% paraformaldehyde for 10 min at RT. On separate sections, $BrdU^+$ cells were also first revealed by rinsing sections in 0.9% NaCl and then incubating them in 2 N HCl for 20 min at 37 °C to denature DNA. The sections were incubated in blocking solution for 20 min at RT and then overnight at 4 °C in rat anti-BrdU (BrdU; 1:500; AbD Serotec, Raleigh, NC). The following day, the sections were incubated in Cy3-conjugated donkey anti-rat IgG (1:500; Jackson Immunoresearch Laboratories, West Grove, PA) for 2 h at RT and then fixed in 4% paraformaldehyde for 10 min at RT.

After revealing EdU^+ or $BrdU^+$ cells, sections were incubated overnight at 4 °C in a cocktail containing 1) the Type-1 NSC and astrocyte marker chicken anti-glial fibrillary acidic protein (GFAP; 1:1000; EnCor Biotechnology, Alachua, FL) and the Type-2a and -2b marker rabbit anti-SOX2 (SOX2; 1:500; Santa Cruz Biotechnology, Santa Cruz, CA), 2) the immature neuronal marker goat anti-doublecortin (DCX; 1:500; Santa Cruz Biotechnology, Santa Cruz, CA) and the mature neuronal marker mouse anti-Neuronal Nuclei (NeuN; 1:500; Chemicon, Temecula, CA), or 3) chicken anti-GFAP (GFAP; 1:1000; EnCor Biotechnology, Alachua, FL) and the oligodendrocyte progenitor marker rabbit anti-NG2 (1:1000; Millipore; Chemicon, Temecula, CA). To phenotype Iba-1^+ cells, sections were incubated in rabbit anti-Iba-1 (1:1000; Wako Chemicals, Wako, TX) and the monocyte/macrophage activation marker CD11b (mouse anti-CD11b; 1:100; Chemicon, Temecula, CA) overnight at 4 °C. After overnight incubation in primary antibodies, all sections were incubated in fully cross-adsorbed cocktails of fluorophore-conjugated secondary antibodies of the appropriate species (1:500; Jackson Immunoresearch, West Grove, PA) for 4 h at RT to reveal primary antibodies. All sections were incubated in 4′,6-diamidine-2′-phenylindole (DAPI; 1:10,000; Calbiochem, San Diego, CA) for 10 min at RT and then mounted under diazobicyclooctane (DABCO; 2.5% DABCO, 10% polyvinyl alcohol and 20% glycerol in TBS).

2.8. Cell counting and stereology

Total $BrdU^+$ and EdU^+ cells were estimated using fractionator principles (Boyce et al., 2010; Kempermann et al., 1997; Noori and Fornal, 2011; Ormerod et al., 2013; Speisman et al., 2013a, b; West et al., 1991). Because $BrdU^+$ and EdU^+ cells are located irregularly and relatively infrequently throughout the subgranular zone and granule cell layer, they were counted exhaustively on every 12th systematically uniform section (240 µm apart) through the rostral-caudal extent of the

dentate gyrus (10 sections per rat) under a 40× objective on a Zeiss Axio Observer Z1 inverted microscope. Only round or oval cells were included in these counts. Total EdU^+ and $BrdU^+$ cell numbers were estimated using the formula $N_{Total} = \Sigma Q^-$ x 1/ssf, where ΣQ^- represents the number of counted cells and ssf is the section sampling fraction (1/12). The average number of dividing $BrdU^+$ cells in sham-kindled (107 ± 7 cells, CV = 0.15, CE = 0.07), and kindled (214 ± 11 cells, CV = 0.11, CE = 0.05) rats and surviving $BrdU^+$ cells in sham-kindled (124 ± 7 cells, CV = 0.13, CE = 0.07) and kindled (235 ± 12 cells, CV = 0.12, CE = 0.05) rats in *Experiment 1*, dividing EdU^+ cells in eGFP (185 ± 13 cells, CV = 0.14; CE = 0.07) and SST-eGFP (159 ± 25 cells, CV = 0.32, CE = 0.16) vector-treated rats and surviving $BrdU^+$ cells in eGFP (233 ± 9 cells, CV = 0.07, CE = 0.04) and SST-eGFP (212 ± 7 cells, CV = 0.06, CE = 0.03) vector-treated rats in *Experiment 2* and dividing $BrdU^+$ cells in eGFP vector-treated (212 ± 13 cells, CV = 0.13, CE = 0.06), SST-eGFP non-responder (177 ± 16 cells, CV = 0.25, CE = 0.09) and SST-eGFP responder (120 ± 10 cells, CV = 0.18, CE = 0.08) rats in *Experiment 3* that were counted was sufficient to ensure reliable estimates between groups (Boyce et al., 2010; Larsen, 1998).

The total number of Iba-1^+ cells was estimated using optical fractionator principles (Bañuelos et al., 2013; Boyce et al., 2010; Ormerod et al., 2013; West et al., 1991). Iba-1^+ cells were counted through the GCL and hilus using Microbrightfield StereoInvestigator software (Williston, VT). Cells were counted on every 12th systematically uniform section (240 µm apart) through the rostral-caudal extent of the dentate gyrus (10 sections per rat) under a 40x objective on a Zeiss Axio Observer Z1 inverted microscope. Iba-1^+ cells were estimated using the formula: $N_{Total} = \Sigma Q^-$ x 1/ssf x 1/asf x *t*/*h*, where ΣQ^- represents the number of counted cells, ssf is the section sampling fraction (1/12), asf is the area sampling fraction or the ratio of the counting frame area to the total area of the fractionator sampling grid (˜1/15 for Iba-1^+ cells), *t* is the average section thickness and *h* is the height of the dissector (0.010 mm). A guard zone of 4 µm was used during Iba-1^+ cell counting to avoid sectioning artifacts. and Iba-1^+ cells in sham-kindled (174 ± 6 cells, CV = 0.17, CE = 0.04) and kindled (225 ± 9, CV = 0.17, CE = 0.04) rats in *Experiment 1*, eGFP (193 ± 9 cells, CV = 0.14; CE = 0.05) and SST-eGFP vector-treated (175 ± 13 cells, CV = 0.21, CE = 0.07) rats in Experiment 2 and in eGFP (206 ± 11 cells, CV = 0.14, CE = 0.05), SST-eGFP responders (217 ± 14 cells, CV = 0.20, CE = 0.06) and SST-eGFP non-responders (211 ± 12 cells, CV = 0.23, CE = 0.06) in *Experiment 3* that were counted was sufficient to ensure reliable stereological estimates (Boyce et al., 2010; Larsen, 1998).

Phenotypic markers were confirmed in each analysis for at least 45 $BrdU^+$ and EdU^+ and at least 100 Iba-1^+ cells in quadruple fluorescent-stained sections under a 20x objective (with 2.5× digital zoom) using a Zeiss LSM 710 meta scanning confocal microscope with 405 nm (to excite DAPI), 488 nm (to excite FITC on non-vector-treated tissue), 510 nm, 543 nm (to excite Cy3), 594 nm (to excite Alexa 594) and 633 nm (to excite Cy5) laser lines. $DAPI^+/BrdU^+$, $DAPI^+/EdU^+$ and $DAPI^+$/Iba-1^+ cells were scanned through their full 'z-dimension' to confirm co-expression of one or more phenotypic marker. Total numbers of cells estimated stereologically were multiplied by the % of cells expressing each phenotype to calculate the total number of dividing Type-1 NSCs ($BrdU^+/GFAP^+/Sox2^+$), dividing Type-2a NPCs ($BrdU^+/GFAP^-/Sox2^+/DCX^-$), dividing Type-2b NPCs ($BrdU^+/GFAP^-/Sox2^+/DCX^+$), new neurons ($BrdU^+$/NeuN+), new astrocytes ($BrdU^+/GFAP^+$), new oligodendrocyte precursors ($BrdU^+/NG2^+$), resting microglia (Iba$1^+/CD11b^-$) and activated microglia (Iba$1^+/CD11b^-$). Percentages of $BrdU^+$ and EdU^+ expressing phenotypic markers are reported in Table 1.

2.9. Statistical analysis

Statistical analyses were performed using Version 13 Statistica software (Tulsa, Oklahoma; rented from http://onthehub.com/). Behavioral variables (number of sessions to the 1st Grade 5 seizure, number of Grade 4/5 seizures, sessions to criterion, AD threshold current) collected prior to vector injection were compared between groups and the effects of the independent variables (kindling and vector treatment) on total EdU^+, $BrdU^+$ or IBA-1^+ cell numbers were tested with analyses of variance (ANOVAs) and revealed by Newman-Keuls post-hoc tests when compared between 3 groups or tested with Student's t-tests when compared between 2 groups. The effects of the independent variables (kindling, vector injection and dentate gyrus subregion) on numbers of dividing cells (Type-1 NSCs, Type-2a NPCs, Type-2b NPCs), numbers of surviving cells (neurons and glia) and numbers of microglia (resting and activated) were tested with repeated measures ANOVAs and revealed by Newman-Keuls post-hoc tests. The effect of vector treatment and AD current increases on test and post-test session seizure grade was assessed using a Mann-Whitney U test for 2 groups or a Kruskal Wallace ANOVA followed by a Mann-Whitney U test for 3 groups. Effect sizes were calculated using Cliff's *d* (Cliff, 1993). Pearson product moment correlation coefficient analyses tested relationships between variables. All figures report means (± S.E.M.). The α-level was set at $p < 0.05$ and reported as two-tailed.

3. Results

3.1. Neurogenesis and microglial activation are potentiated in the hippocampi of kindled rats

In *Experiment 1*, we tested whether the number and phenotype of $BrdU^+$ cells and the number and activation state of Iba-1^+ microglia varied in the hippocampi of sham-kindled and kindled rats that were injected with BrdU 48 h after kindled rats achieved criterion and then perfused either 4 h or 4 weeks later (see Fig. 1). The average AD threshold current employed during kindling sessions was 205.0 ± 15.7 µA and kindled rats exhibited their 1st Grade 5 seizure after 13.8 ± 1.8 sessions (˜7 d), exhibited 5.5 ± 0.8 high-grade seizures during kindling sessions and achieved kindling criterion after 18.5 ± 1.8 sessions (˜9 d).

3.1.1. More dividing Type-1 NSCs and activated microglial were detected in the hippocampi of kindled rats

To test the effects of kindling on the number of Type-1 NSCs, Type-2 NPCs and activated microglia, rats were injected with BrdU 48 h after kindled rats achieved criterion and then perfused 4 h after BrdU injection. Fig. 3 shows a representative microphotograph of DAB-stained dividing $BrdU^+$ cells (in brown) in the dentate gyrus of **(A)** a kindled rat (the inset shows $BrdU^+$ cells under 63x magnification) and **(B)** a sham-kindled rat. Fig. 3**C** shows a representative confocal image of DAPI-stained (in gray) dividing $BrdU^+$ (in red) cells expressing the Type-1 NSC marker GFAP (in cyan) and/or the Type-2 NPC marker SOX2 (in green). The Fig. 3**C** insets show examples of Type-1 $GFAP^+/SOX2^+$ NSCs (yellow arrows) and a Type-2 $GFAP^-/SOX2^+$ NPC (white arrow) in single detection channels for each signal.

Fig. 3**D** shows that the mean (± S.E.M.) total number of dividing $BrdU^+$ cells was significantly higher in the dentate gyri of kindled versus sham-kindled rats ($t_{(8)} = 8.26$; $p < 0.001$***). Fig. 3**E** shows the total number of dividing Type-1 NSCs, Type-2a NPCs and Type-2b NPCs in the dentate gyri of sham-kindled and kindled rats. Note that because similarly rare $BrdU^+$ cells expressed Type-3 neuroblast phenotypes in either sham-kindled or kindled rats 4 h after BrdU injection (< 1% in either group), they were excluded from further analyses (see Table 1 for percentages of $BrdU^+$ cells expressing each phenotype). The total number of dividing cells varied by phenotype ($F_{(2,16)} = 26.47$; $p < 0.001$), group ($F_{(1,8)} = 51.50$; $p < 0.001$) and the interaction between phenotype and group ($F_{(2,16)} = 10.00$; $p < 0.001$). Overall, more dividing cells were found in the dentate gyri of kindled versus sham-kindled rats ($p < 0.001$) and generally, most dividing cells were Type-

Table 1
The % of $BrdU^+$ and EdU^+ cells expressing phenotypic markers.

	Type-1 NSC ($GFAP^+/Sox2^+$)	Type-2a NPC ($GFAP^-/Sox2^+$)	Type-2b NPC ($Sox2^+/DCX^+$)	Immature Neuron (DCX^+)	Transition Neuron ($DCX^+/NeuN^+$)	Mature Neuron ($NeuN^+$)	Astrocyte ($GFAP^+$)
Experiment 1							
Sham-kindled	38.5 ± 3.2	58.0 ± 1.8	11.0 ± 3.4	1.4 ± 0.6	20.7 ± 2.3	54.0 ± 5.4	8.1 ± 2.1
Kindled	58.2 ± 4.4	38.9 ± 4.4	7.1 ± 3.2	4.0 ± 1.2	13.5 ± 4.2	65.0 ± 5.5	0.8 ± 0.4
Experiment 2							
eGFP vector-treated	63.3 ± 4.5	32.9 ± 4.2		2.4 ± 1.9	2.5 ± 0.4	82.1 ± 4.7	2.5 ± 0.5
SST-eGFP vector-treated	59.7 ± 5.6	34.0 ± 5.4		1.6 ± 1.1	3.1 ± 1.4	81.2 ± 2.2	7.4 ± 2.5
Experiment 3							
eGFP vector-treated	54.0 ± 0.6	40.9 ± 1.1		–	–	–	–
SST-eGFP NR	64.5 ± 1.8	32.3 ± 1.8		–	–	–	–
SST-eGFP R	39.6 ± 4.4	55.6 ± 4.0		–	–	–	–

1 NSCs ($p < 0.01$ versus Type-2a and $p < 0.001$ versus -2b NPCs) followed by Type-2a NPCs ($p < 0.001$ versus Type-2b NPCs). The latter effect was primarily due to the increased number of dividing Type-1 NSCs in the dentate gyri of kindled versus sham-kindled rats ($p < 0.001$***). In fact, while similar numbers of dividing Type-1 NSCs and -2a NPCs were found in the dentate gyri of sham-kindled rats, dividing Type-1 NSCs outnumbered dividing Type-2a NPCs in kindled rats ($p < 0.001$***). Because the number of dividing Type-2a and Type-2b NPCs were not affected by kindling, these cell numbers were pooled in *Experiment 2* and *3*. These data show that the number of Type-1 NSCs is upregulated in the dentate gyri of kindled rats.

Fig. 3**F** shows a representative photomicrograph of DAB-stained Iba-1^+ microglia (in brown; the inset shows Iba-1^+ cells under 63x magnification). Representative confocal images of a DAPI-labeled (in gray) resting $CD11b^-$/Iba-1^+ (in cyan) microglia and a DAPI-labeled activated $CD11b^+$ (in green)/Iba-1^+ (in cyan) microglia in the dentate gyrus of a kindled rat are shown in Fig. 3**G** and **H**, respectively. The insets show each signal in single detection channels. Iba-1^+/$CD11b^-$ microglia exhibited classic resting morphologies with small round cell bodies and extensive branching while Iba-1^+/$CD11b^+$ microglia exhibited classic activated morphologies with larger cell bodies and shorter, thicker cell processes. Fig. 3**I** shows the mean (± S.E.M.) total number of Iba-1^+ microglia in the GCL and hilus of sham-kindled and kindled rats. In both groups combined, more Iba-1^+ microglia were found in the hilus than GCL of all rats combined ($F_{(1,8)} = 6.81$; $p < 0.05$*), but microglia numbers neither varied by group ($F_{(1,8)} = 3.95$; $p = 0.08$) nor by the overall interaction ($F_{(1,8)} = 0.01$; $p = 0.93$). Fig. 3**J** shows the mean (± S.E.M.) total number of Iba-1^+ microglia expressing $CD11b^-$ resting versus $CD11b^+$ activated states in the GCL and hilus of sham-kindled and kindled rats. The total number of microglia varied region ($F_{(1,8)} = 6.81$; $p < 0.05$), the interaction between group and activation state ($F_{(1,8)} = 105.24$; $p < 0.0001$) and the overall interaction ($F_{(1,8)} = 11.29$; $p < 0.01$) but did not vary by group, activation state or other interactions between the independent variables (all *p values* $\geq$ 0.08). In both groups combined, more microglia were found in the hilus versus GCL ($p < 0.05$). However, the number of resting microglia was lower while the number of activated microglia was higher in the GCL ($p < 0.01$** and $p < 0.001$***, respectively) and hilus (both *p values* < 0.001***) of kindled versus sham-kindled rats. In sham-kindled rats, more resting versus activated microglia were found in both the GCL ($p < 0.01^a$) and hilus ($p < 0.001^a$). In these rats, ratios of activated versus resting microglia were 0.48 in the GCL and 0.95 in the hilus and the ratio of activated microglia in the hilus versus GCL was 0.95. In kindled rats, more activated than resting microglia were found in the GCL ($p < 0.001^b$) and hilus ($p < 0.001^b$), and the number of activated microglia was elevated in the hilus versus GCL ($p < 0.05^c$). In these rats, ratios of activated versus resting microglia were 2.28 in the GCL and 3.97 in the hilus and the ratio of activated microglia in the hilus versus GCL was 1.25. These data demonstrate that numbers of activated microglia are increased in the GCL and more robustly in the hilus of kindled rats, just after their last Grade 5 seizure.

The total number of dividing Type-1 NSCs correlated positively with the total number of activated GCL ($r_{(10)} = 0.90$; $p < 0.0001$) and hilar ($r_{(10)} = 0.80$; $p < 0.01$) microglia and negatively with the total number of resting GCL ($r_{(10)} = -0.85$; $p < 0.01$) and hilar ($r_{(10)} = -0.75$; $p < 0.05$) microglia. Numbers of dividing Type-2 NPCs were unrelated to numbers of dividing Type-1 NSCs, resting microglia or activated microglia. These data suggest that microglial activation and Type-1 NSC proliferation may be related processes in the hippocampi of kindled rats.

3.1.2. Microglial activation persists for several weeks in the hippocampi of kindled rats

To test whether NSCs and NPCs that divide in the hippocampi of kindled rats produce similar numbers of surviving neurons and glia and whether kindling produces a persistent microglial response, rats were injected with BrdU 48 h after achieving criterion and then perfused 4 weeks later (see Fig. 1). Fig. 4**A** shows a representative confocal image of a 4 week-old $BrdU^+$ cell (in red) expressing the mature neuronal protein $NeuN^+$ (in green). Immature DCX^+ neurons (in cyan) and transitioning $NeuN^+/DCX^+$ neurons are also shown. Fig. 4**B** shows a representative confocal image of a 4 week-old $BrdU^+$ cell (in red) expressing the astrocyte protein GFAP (in cyan). $NG2^+$ oligodendrocyte precursor cells are shown in green. Because less than 1% of $BrdU^+$ cells expressed NG2 in the dentate gyri of either sham-kindled or kindled rats, new oligodendrocyte precursors were excluded from further analyses.

Fig. 4**C** shows that the total number of surviving 4 week-old $BrdU^+$ cells was significantly higher in the hippocampi of kindled versus sham-kindled rats ($t_{(8)} = 7.77$; $p < 0.0001$***). Fig. 4**D** shows the mean (± S.E.M.) total number of new $BrdU^+$ astrocytes and neurons expressing immature, transitioning and mature phenotypes (see Table 1 for the percentages of $BrdU^+$ cells expressing each phenotype). This number varied by group ($F_{(1,8)} = 28.76$; $p < 0.001$), phenotype ($F_{(3,24)} = 60.99$; $p < 0.001$), and the overall interaction ($F_{(3,24)} = 11.52$; $p < 0.001$). A greater number of differentiated $BrdU^+$ cells was found in the hippocampi of kindled versus sham-kindled rats ($p < 0.001$), primarily because more mature new neurons were found in kindled versus sham-kindled rats ($p < 0.001$***). Irrespective of group and consistent with a 4-week survival period, most new cells had differentiated into mature neurons ($p < 0.001^a$ versus all other phenotypes) followed by transitioning neurons ($p \leq 0.05^b$ versus immature neurons and astrocytes). In the dentate gyri of kindled versus sham-kindled rats, the 2.1-fold increase in total new neuron number detected 4 weeks after BrdU reflected the 2-fold increase in

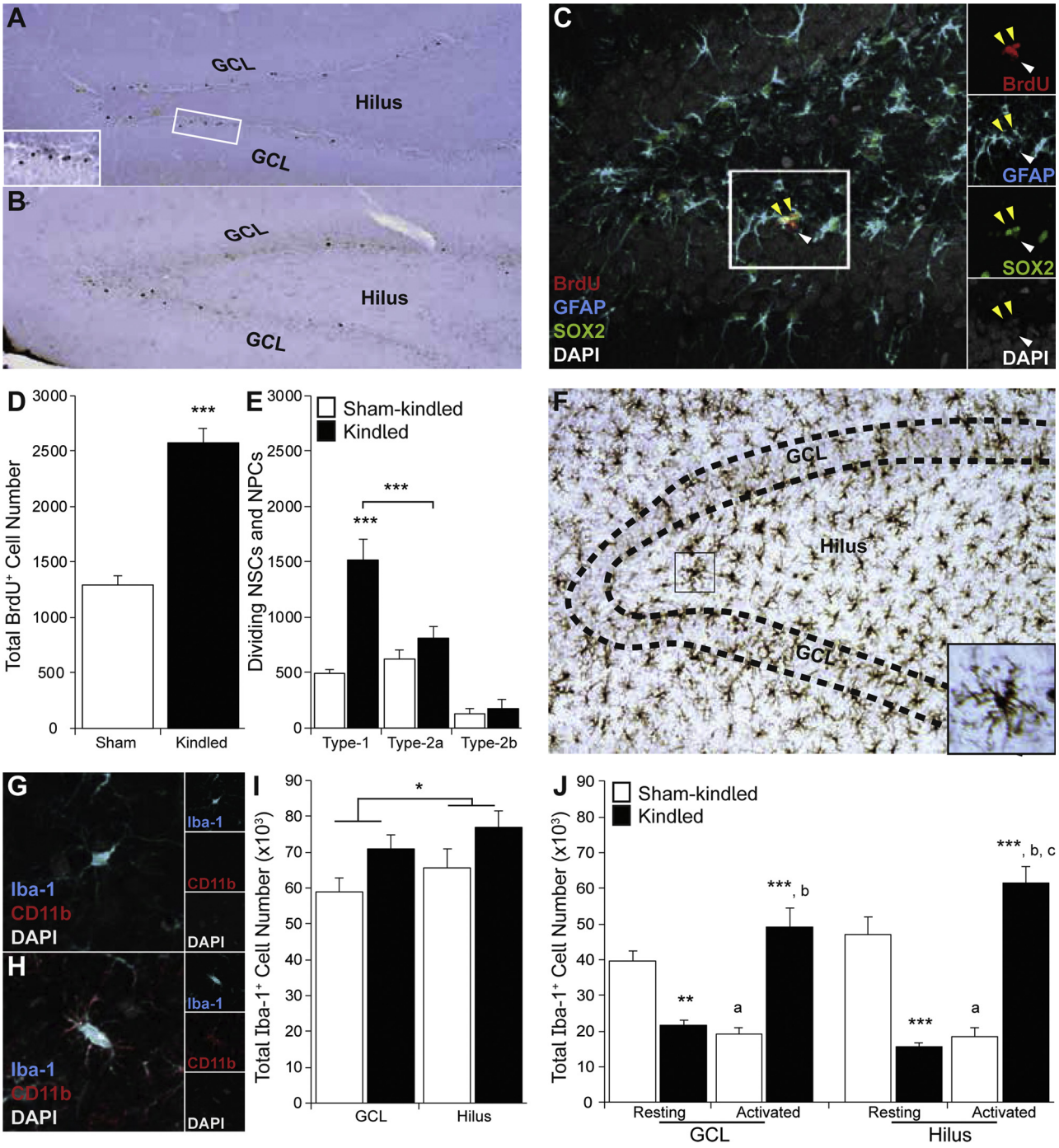

Fig. 3. The number of dividing Type-1 neural stem cells and activated microglia was increased in the hippocampi of kindled rats. Representative microphotographs of DAB-stained dividing BrdU$^+$ cells (in brown) in the dentate gyrus of a kindled **(A)** and sham-kindled **(B)** rat. **(C)** Representative fluorescent image of dividing BrdU$^+$/Sox2$^+$/GFAP$^+$ Type-1 NSCs (yellow arrowheads) and a BrdU$^+$/Sox2$^+$/GFAP$^-$ Type-2 NPC (white arrowhead). **(D)** Stereological estimates of BrdU$^+$ cells within the DG revealed a ˜2-fold increase in proliferation ($p < 0.001$***) 48 h after rats reached kindling criterion. **(E)** More BrdU$^+$ Type-1 NSCs were found in the dentate gyri of kindled versus sham-kindled rats ($p < 0.001$***) and in kindled rats, more dividing Type-1 NSCs were detected than Type-2 NPCs ($p < 0.001$***). **(F)** Representative microphotograph of DAB-stained Iba-1$^+$ microglia (in brown) in the dentate gyrus. **(G, H)** Representative fluorescent images of a resting Iba-1$^+$/CD11b$^-$ microglia **(G)** and activated Iba-1$^+$/Cd11b$^+$ microglia **(H)**. **(I)** Stereological estimates revealed similar Iba-1$^+$ microglia numbers in the granule cell layer and hilus of kindled and sham-kindled rats but more Iba-1$^+$ microglia were found in the hilus versus granule cell layer of all rats ($p < 0.05$*), **(J)** however, fewer resting microglia were found in the GCL ($p < 0.01$**) and hilus ($p < 0.001$***) of kindled versus sham-kindled rats that had a greater number of activated microglia in the GCL ($p < 0.001$***) and hilus ($p < 0.001$***). In sham-kindled rats, more resting than activated microglia were found in both the GCL ($p < 0.01^a$) and hilus ($p < 0.001^a$). In kindled rats, more activated than resting microglia were found in the GCL ($p < 0.001^b$) and hilus ($p < 0.001^b$) and the number of activated microglia was elevated in the hilus versus GCL ($p < 0.05^c$).

dividing cells detected at 4 h after BrdU, suggesting that increased new neuron numbers are a function of increased numbers of dividing cells rather than changes in the differentiation or survival of new neurons.

Fig. 4**E** shows the mean (± S.E.M.) total number of Iba-1$^+$ microglia in the GCL and hilus of sham-kindled and kindled rats 4 w after their last kindling session (see Fig. 3**F** for examples of Iba-1$^+$

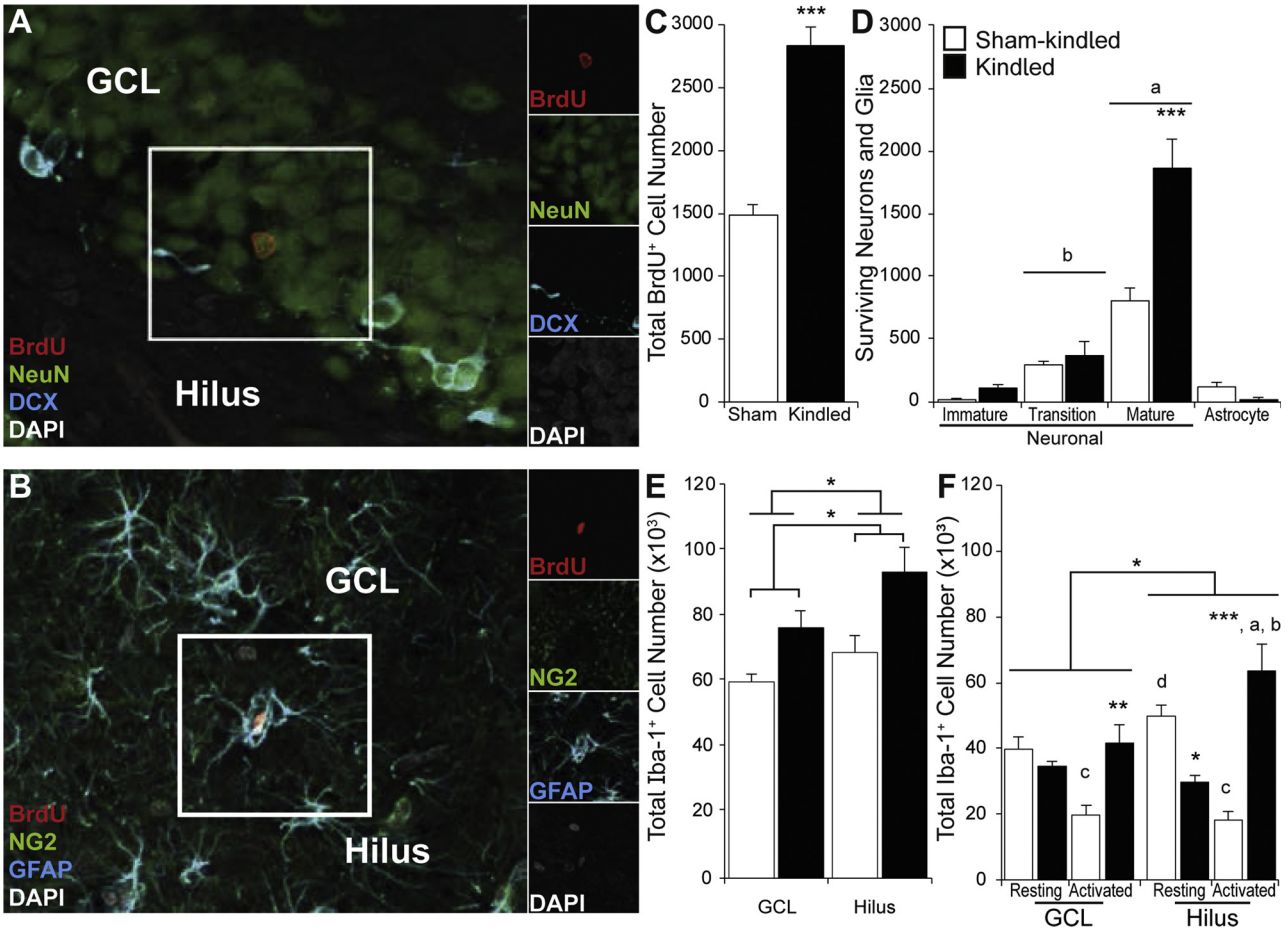

Fig. 4. Kindling increases the number of surviving neurons and leads to persistent microglial activation. Representative fluorescent images of a new adult-born $BrdU^+/NeuN^+$ granule neuron **(A)** and $BrdU^+/GFAP^+$ astrocyte **(B)**. **(C)** Stereological estimate of surviving ($BrdU^+$) cells revealed a ~2-fold increase in the number of surviving cells in kindled rats ($p < 0.001$***) at 4 weeks after reaching kindling criterion and BrdU injection. **(D)** Quantification of the number of surviving immature ($BrdU^+/DCX^+/NeuN^-$), transitioning ($BrdU^+/DCX^+/NeuN^+$), mature ($BrdU^+/DCX^-/NeuN^+$) neurons, and astrocytes ($BrdU^+/GFAP^+$) revealed that kindling increased the number of mature neurons relative to sham-kindling ($p < 0.001$***) and consistent with other reports and our timeline, the majority of newly-born cells differentiated into neurons with most having reached the mature phenotype ($p < 0.001^a$ versus all other phenotypes, followed by transitioning neurons ($p \leq 0.05^b$ versus immature neurons and astrocytes). **(E)** Stereological estimates for total microglia ($Iba\text{-}1^+$) within the GCL and hilus revealed more microglia in both regions in kindled rats versus sham-kindled and more micrglia in the hilus versus GCL of all rats (*p values* < 0.05*). **(F)** Quantification of resting and activated microglia in the GCL and hilus revealed no difference in the number of resting microglia in the GCL between groups but fewer resting in the hilus of kindled versus sham-kindled rats ($p < 0.05$*). There were more activated microglia in both the GCL ($p < 0.001$**) and the hilus ($p < 0.001$***) of kindled rats versus sham-kindled. There were more microglia in the hilus versus GCL of all rats ($p < 0.05$*). In kindled rats, more activated microglia were found in the hilus versus GCL ($p < 0.001^a$) and in the hilus, activated microglia outnumbered resting microglia ($p < 0.001^b$). In sham-kindled rats, fewer activated than resting microglia were found in the GCL ($p < 0.01^c$) and hilus ($p < 0.001^c$) and more resting microglia were found in the hilus versus GCL ($p \leq 0.05^d$).

Table 2
The % of $Iba\text{-}1^+$ microglia expressing phenotypic markers.

	Granule Cell Layer		Hilus	
	Resting Microglia ($Iba\text{-}1^+/CD11b^-$)	Activated Microglia ($Iba\text{-}1^+/CD11b^+$)	Resting Microglia ($Iba\text{-}1^+/CD11b^-$)	Activated Microglia ($Iba\text{-}1^+/CD11b^+$)
Experiment 1				
Sham-kindled (4 h survival)	67.2 ± 2.0	32.8 ± 2.0	71.7 ± 3.0	28.3 ± 3.0
Kindled (4 h survival)	31.3 ± 3.8	68.7 ± 3.8	20.4 ± 1.6	79.6 ± 1.6
Sham-kindled (4 w survival)	66.4 ± 4.9	33.6 ± 4.9	72.6 ± 1.7	27.4 ± 1.7
Kindled (4 w survival)	46.0 ± 3.5	54.0 ± 3.5	33.1 ± 3.9	66.9 ± 3.9
Experiment 2				
eGFP vector-treated	31.7 ± 4.9	68.3 ± 4.9	20.4 ± 3.1	79.6 ± 3.1
SST-eGFP vector-treated	31.3 ± 2.2	68.7 ± 2.2	20.2 ± 3.7	79.8 ± 3.7
Experiment 3				
eGFP vector-treated	38.0 ± 4.6	62.0 ± 4.6	30.5 ± 3.2	69.5 ± 3.2
SST-eGFP NR	40.9 ± 2.8	59.1 ± 2.8	19.1 ± 1.7	80.9 ± 1.7
SST-eGFP R	40.4 ± 2.9	59.6 ± 2.9	22.1 ± 2.5	77.9 ± 2.5

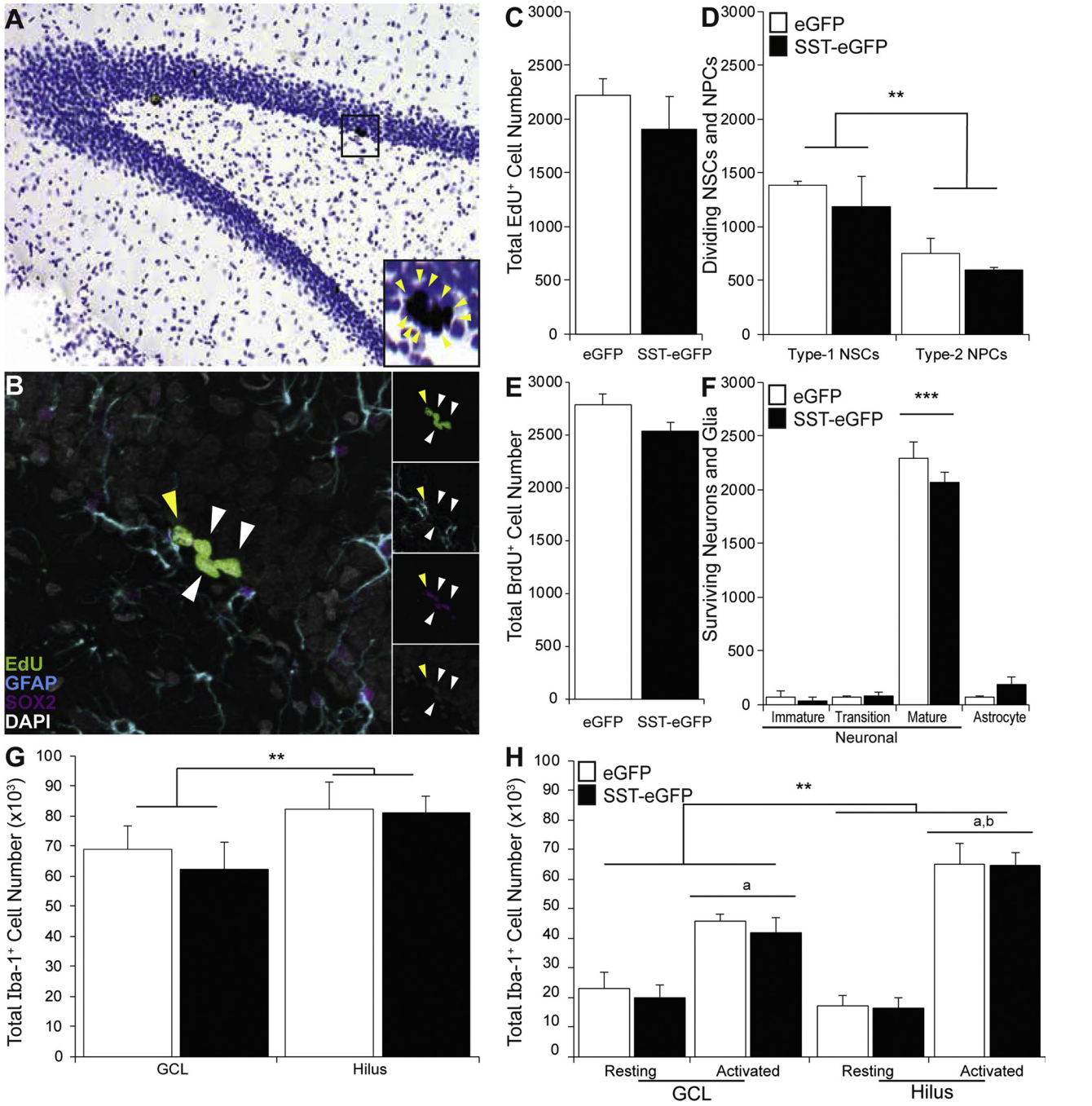

Fig. 5. Sustained SST transgene expression did not impact dividing, surviving cells, or microglial response in kindled rats. (A) Representative photomicrograph of DAB-stained dividing EdU^+ cells under a 10X objective with an inset of a cluster of newly dividing/divided cells under 63X magnification. **(B)** Representative fluorescent image of newly divided $EdU^+/Sox2^+$ Type-2 NPCs in the GCL of kindled rats. **(C)** Stereological estimates for newly divided (EdU^+) cells revealed no significant difference in dividing cell number between eGFP- and SST-eGFP vector-treated rats. **(D)** Quantification of the number of newly divided Type-1 NSCs and Type-2 NPCs revealed no differences between eGFP- and SST-eGFP vector-treated rats 2d after their last post-test stimulation but more Type-1 NSCs than Type-2 NPCs in both groups combined ($p < 0.01$**) **(E)** Stereological estimates for surviving ($BrdU^+$) cells revealed no difference 6 weeks after vector-treated rats achieved kindling criterion and received their respective vector injections. **(F)** Quantification of the phenotype (immature $DCX^+/NeuN^-$ neuron, transitioning $DCX^+/NeuN^+$ neuron, mature $DCX^-/NeuN^+$ neuron, or $GFAP^+$ astrocyte) of surviving cells revealed no difference between treatment groups 6 weeks after treated rats reached kindling criterion and received their respective vector injections, but more mature neurons were found versus all other cell types in both groups combined ($p < 0.001$***). **(G)** Stereological estimates of total microglia ($Iba\text{-}1^+$) within the GCL and hilus revealed no differences between treatment groups on microglia phenotype in the GCL or hilus but more microglia were found in the hilus versus GCL of both groups combined ($p < 0.01$**). **(H)** In both groups combined, hilar microglia outnumbered GCL microglia ($p < 0.01$**), the number of activated microglia outnumbered resting microglia in the GCL ($p < 0.01^a$) and the hilus ($p < 0.001^a$) and the number of activated microglia was higher in the hilus versus GCL ($p < 0.01^b$). These data show that SST-eGFP vector-treatment did not reverse the kindling-induced activation of microglia.

microglia). This number varied by group ($F_{(1,8)} = 10.24$; $p < 0.05$) and region ($F_{(1,8)} = 11.06$; $p < 0.05$) but not by the overall interaction ($F_{(1,8)} = 1.02$; $p = 0.34$). More microglia were detected in kindled versus sham-kindled rats ($p < 0.05$*) and more microglia were found in the hilus versus GCL ($p < 0.05$*) of both groups combined. Fig. 4**F** shows the mean (± S.E.M.) total number of resting and activated

microglia in the GCL and hilus of sham-kindled and kindled rats (see Table 2 for percentages of Iba-1$^+$ cells expressing the activation marker CD11b). This number varied by group ($F_{(1,8)} = 10.70$; $p < 0.05$), region ($F_{(1,8)} = 11.43$; $p < 0.01$), the interaction between activation state and group ($F_{(1,8)} = 28.27$; $p < 0.001$) and the overall interaction ($F_{(1,8)} = 29.20$; $p < 0.001$), but not by activation state or other interactions between the independent variables (all p *values* $\geq$ 0.07). More microglia were found in the hippocampi of kindled versus sham-kindled rats ($p < 0.05$) and in the hilus versus GCL of both groups combined ($p < 0.01$**). More activated microglia were found in the GCL and hilus of kindled versus sham-kindled rats ($p < 0.01$** and $p < 0.001$***, respectively) and fewer resting microglia were found in the hilus of kindled versus sham-kindled rats ($p < 0.05$). In kindled rats, more activated microglia were found in the hilus versus GCL ($p < 0.001^a$) and in the hilus, activated microglia outnumbered resting microglia ($p < 0.001^b$). In these rats, the ratio of activated versus resting microglia was 1.21 in the GCL and 2.13 in the hilus and the ratio of activated microglia in the hilus versus GCL was 1.52. In sham-kindled rats, fewer activated than resting microglia were found in the GCL ($p < 0.01^c$) and hilus ($p < 0.001^c$) and more resting microglia were found in the hilus versus GCL ($p \leq 0.05^d$). In these rats, the ratio of activated versus resting microglia was 0.50 in the GCL and 0.37 in the hilus and the ratio of activated microglia in the hilus versus GCL was 0.92. The data demonstrate that increased numbers of activated microglia can be detected in the hippocampi of kindled rats for at least 4 weeks after they exhibit their final Grade 5 seizure and that the effects are most robust in the hilus.

Total mature new neuron number correlated positively with total new neuron number ($r_{(10)} = 0.96$; $p < 0.0001$) and total new neuron number correlated positively with the total number of activated hilar microglia ($r_{(10)} = 0.65$; $p < 0.05$) and negatively with the total number of resting hilar microglia ($r_{(10)} = -0.74$; $p < 0.05$). Since similar fold-increases in surviving new neurons and dividing Type-1 NSCs were detected in the dentate gyri of kindled versus sham-kindled rats, the relationship between persistently activated hilar microglia and mature new neuron numbers could instead reflect the relationship between activated hilar microglia and dividing Type-1 NSC numbers.

3.2. Sustained SST expression neither affected neurogenesis nor microglial activation in a small cohort of kindled rats

Experiment 2 tested whether vector-mediated sustained SST expression could alter the effects of amygdala kindling on the number and phenotype of dividing EdU$^+$ cells, surviving BrdU$^+$ cells and Iba-1$^+$ microglia in the hippocampi of rats. Kindled rats were injected with BrdU 48 h after reaching criterion and then infused intrahippocampally with eGFP or SST-eGFP vector. Three weeks later, they were given a test stimulation followed by post-test stimulations. The rats were injected with EdU 48 h after the final post-test stimulation and perfused 4 h later (see Fig. 1).

Before assignment to vector treatment groups, eGFP- and SST-eGFP vector-treated rats exhibited similar AD threshold currents (eGFP: 200.0 ± 35.4 μA and SST-eGFP: 137.5 ± 12.5 μA; $t_{(6)} = -1.67$; $p = 0.15$), exhibited their first Grade 5 seizure after a similar number of sessions (eGFP: 16.3 ± 1.1 sessions and SST-eGFP: 12.5 ± 2.9 sessions; $t_{(6)} = -1.21$; $p = 0.27$), exhibited similar numbers of high-grade seizures (eGFP: 5.8 ± 0.6 seizures and SST-eGFP: 5.0 ± 1.1 seizures; $t_{(6)} = -0.60$; $p = 0.57$) and required similar numbers of sessions to achieve criterion (eGFP: 21.3 ± 1.8 sessions and SST-eGFP: 16.3 ± 4.2 sessions; $t_{(6)} = -1.08$, $p = 0.32$). Although 2/4 SST-eGFP vector-treated rats exhibited Grade 0 seizures on the test session administered 3 weeks after vector injection, both groups exhibited similar average seizure grades on the test session (eGFP 3.5 ± 1.2 and SST-eGFP: 1.3 ± 1.0; $U = 3.50$, $n_1 = n_2 = 4$, $p = 0.25$) and similar average seizure grades across post-test sessions (eGFP: 2.8 ± 1.1 and SST-eGFP: 3.6 ± 0.7; $U = 8.00$, $n_1 = n_2 = 4$, $p = 1.00$). Although we did not observe an effect of SST-eGFP vector treatment on seizure behavior in *Experiment 2*, we were interested in testing whether SST-eGFP vector treatment produced independent effects upon neurogenesis and microglial activation in kindled rats.

Fig. 5**A** shows a representative microphotograph of DAB-stained EdU$^+$ cells and the inset shows a cluster of EdU$^+$ cells under 63x magnification. Fig. 5**B** shows a representative confocal image of dividing EdU$^+$ cells (in green) expressing the Type-1 NSC marker GFAP (in cyan) and the Type-2 NPC marker SOX2 (in pink) counted 4 h after EdU injection. The insets show examples of Type-1 GFAP$^+$/SOX2$^+$ NSCs (yellow arrow) and Type-2 GFAP$^-$/SOX2$^+$ NPCs (white arrows). Fig. 5**C** shows that the total number of dividing EdU$^+$ cells was similar in the hippocampi of SST-eGFP versus eGFP vector-treated rats ($t_{(6)} = 0.92$; $p = 0.39$). Fig. 5**D** shows the mean (± S.E.M.) total number of dividing EdU$^+$ Type-1 NSCs and Type-2 NPCs in the hippocampi of kindled rats treated with eGFP or SST-eGFP vector (see Table 1 for the percentages of EdU$^+$ cells expressing each phenotype). While more Type-1 NSCs were observed than Type-2 NPCs ($F_{(1,6)} = 14.25$; $p < 0.01$**), these numbers neither varied by group ($F_{(1,6)} = 1.16$; $p = 0.32$) nor the overall interaction ($F_{(1,6)} = 0.02$; $p = 0.88$). Fig. 5**E** shows that the mean (± S.E.M.) total number of surviving BrdU$^+$ cells was similar in the hippocampi of eGFP- and SST-eGFP vector-treated rats ($t_{(6)} = -1.95$; $p = 0.10$). Fig. 5**F** shows the mean (± S.E.M.) net numbers of surviving BrdU$^+$ neurons and astrocytes in the hippocampi of eGFP and SST-eGFP vector-treated rats. These numbers varied by phenotype ($F_{(3,18)} = 317.14$; $p < 0.0001$), but not by group ($F_{(1,6)} = 0.57$; $p = 0.48$) or the overall interaction ($F_{(3,18)} = 1.80$; $p = 0.18$). In both groups combined, the majority of surviving BrdU$^+$ cells were mature neurons ($p < 0.001$*** versus all other phenotypes). Taken together, these data show that there was no effect of SST-eGFP vector treatment on surviving BrdU$^+$ cells or on dividing EdU$^+$ cells in the dentate gyri of kindled rats. However, dependent t-tests confirmed that while numbers of surviving BrdU$^+$ and dividing EdU$^+$ cell numbers were related in eGFP vector-treated rats ($t_{(3)} = 8.68$; $p < 0.01$), they were unrelated in SST-eGFP vector-treated rats ($t_{(3)} = 1.68$; $p = 0.19$). In combination with our *Experiment 1* observation that similar fold increases in dividing Type-1 NSCs and surviving neurons are detected in kindled rats (Figs. 3**D** and 4 C), these data suggest that SST-eGFP vector treatment increased within-subjects variability enough to mask the relationship between the number of dividing cells labeled with BrdU before and EdU after SST-eGFP vector treatment.

Fig. 5**G** shows the mean (± S.E.M.) total number of microglia in the GCL and hilus of eGFP- and SST-eGFP-vector-treated rats. Although more Iba-1$^+$ microglia were found in the hilus versus GCL ($F_{(1,6)} = 30.55$; $p < 0.01$**), this number neither varied by group ($F_{(1,6)} = 0.13$; $p = 0.73$) nor the overall interaction ($F_{(1,6)} = 1.04$; $p = 0.35$). Fig. 5**H** shows the mean (± S.E.M.) numbers of resting and activated Iba-1$^+$ microglia in the GCL and hilus of eGFP- and SST-eGFP vector-treated rats (see Table 2 for percentages of Iba-1$^+$ microglia that expressed the activation marker CD11b). These numbers varied by region ($F_{(1,6)} = 30.55$; $p < 0.01$), activation state ($F_{(1,6)} = 319.26$; $p < 0.0001$) and the interaction between region and activation state ($F_{(1,6)} = 21.89$; $p < 0.01$) but not by group or other interactions between the independent variables (all p *values* $\geq$ 0.35). In both groups combined, hilar microglia outnumbered GCL microglia ($p < 0.01$**), activated microglia outnumbered resting microglia ($p < 0.001$), the number of activated microglia outnumbered resting microglia in the GCL ($p < 0.01^a$) and the hilus ($p < 0.001^a$) and the number of activated microglia was higher in the hilus versus GCL ($p < 0.01^b$). The ratio of activated versus resting microglia was 2.05 in the GCL and the 3.86 in the hilus and the ratio of activated microglia in the hilus versus GCL was 1.47. These data show that SST-eGFP vector treatment did not reverse the kindling-induced activation of microglia.

In vector-treated rats, the total number of activated hilar microglia correlated positively with the numbers of resting ($r_{(8)} = 0.86$; $p <$

0.01) and activated GCL microglia ($r_{(8)} = 0.74$; $p < 0.05$) but negatively with mature new neuron numbers ($r_{(8)} = -0.75$; $p < 0.05$). In the GCL, numbers of activated and resting microglia were correlated positively ($r_{(8)} = 0.87$; $p < 0.01$). These correlations suggest that an inflammatory response persists most profoundly in the dentate gyri of kindled rats and that the severity of microglial activation may influence the survival of new neurons.

3.3. Sustained SST expression reverses kindling-induced changes in NSC proliferation and potentiates activated microglia numbers in behavioral responders

Since we previously demonstrated that subsets of rats respond behaviorally to sustained SST expression (Natarajan et al., 2017), we kindled a larger cohort of rats to test whether sustained SST expression differentially impacts neurogenesis and neuroinflammation in behavioral responders and non-responders. Rats were kindled to criterion, treated with eGFP or SST-eGFP vector and then given a test session followed by post-test sessions after a 3-week recovery. Rats were injected with BrdU 48 h after their final post-test session and perfused 4 h later (see Fig. 1).

A subset of rats in the SST-eGFP vector-treated group responded to treatment by exhibiting Grade 0 seizures on the test session while others exhibited high grade seizures. We therefore divided the SST-eGFP vector-treated group into SST-eGFP vector-treated responder (n = 5) and SST-eGFP vector-treated non-responder (n = 8) groups. Prior to vector treatment, the eGFP vector-treated controls, SST-eGFP vector-treated responders and non-responders exhibited similar AD threshold currents (eGFP vector-treated controls: 187.5 ± 12.5 μA, SST-eGFP responders: 230.0 ± 33.9 μA, SST-eGFP non-responders: 212.5 ± 32.4 μA; $F_{(2,14)} = 0.34$; $p = 0.72$), numbers of sessions before exhibiting their first Grade 5 seizure (eGFP vector-treated controls: 20.0 ± 3.1 sessions, SST-eGFP responders: 18.4 ± 2.3 sessions, and SST-eGFP non-responders: 16.5 ± 1.8 sessions; $F_{(2,14)} = 0.60$; $p = 0.56$), numbers of high-grade seizures (eGFP vector-treated controls: 9.3 ± 2.0 seizures and SST-eGFP responders: 5.4 ± 0.9 seizures and SST-eGFP non-responders: 7.1 ± 1.0 seizures; $F_{(2,14)} = 1.85$; $p = 0.19$) and numbers of sessions to achieve criterion (eGFP vector-treated controls: 27.0 ± 2.1 sessions, SST-eGFP responders: 23.0 ± 2.3 sessions, and SST-eGFP non-responders: 22.6 ± 1.7 sessions; $F_{(2,14)} = 1.18$, $p = 0.35$). We found a significant effect of vector treatment on test session seizure grade (eGFP vector-treated controls: 3.3 ± 0.9, SST-eGFP responders: 0.0 ± 0.0 and SST-eGFP non-responders: 4.9 ± 0.1; $H_{(2,17)} = 12.72$; $p < 0.01$), such that SST-eGFP responders exhibited a lower seizure grade than either eGFP vector-treated controls ($p < 0.05$) and SST-eGFP non-responders ($p < 0.01$). The effect size of the difference between the eGFP vector-treated and SST-eGFP responder groups on test session seizure grade ($d = 2.47$) far exceeded Cliff's convention for a large effect size (Cliff, 1993). We tested average post-test session grade prior to stepping up the AD current as a measure of therapeutic resilience and found a significant effect of vector treatment (eGFP vector-treated controls: 4.6 ± 0.3, SST-eGFP responders: 1.6 ± 0.9, SST-eGFP non-responders: 4.8 ± 0.1; $H_{(2,17)} = 6.73$; $p < 0.05$), such that SST-eGFP responders exhibited a lower average seizure grade across post-test sessions than SST-eGFP non-responders ($p < 0.05$). Group differences were not detected at higher stimulation currents.

Fig. 6**A** shows that the mean (± S.E.M.) total number of dividing BrdU$^+$ cells differed in the hippocampi of eGFP vector-treated controls, SST-eGFP responders and SST-eGFP non-responders ($F_{(2,14)} = 7.84$; $p < 0.01$), such that SST-eGFP responders had fewer dividing BrdU$^+$ cells than either eGFP vector-treated controls ($p < 0.01^a$) or SST-eGFP non-responders ($p < 0.05^b$). Fig. 6**B** shows the mean (± S.E.M.) total number of dividing BrdU$^+$ Type-1 NSCs and Type-2 NPCs in the hippocampi of eGFP vector-treated controls, SST-eGFP non-responders, and SST-eGFP responders (see Table 1 for the percentages of BrdU$^+$

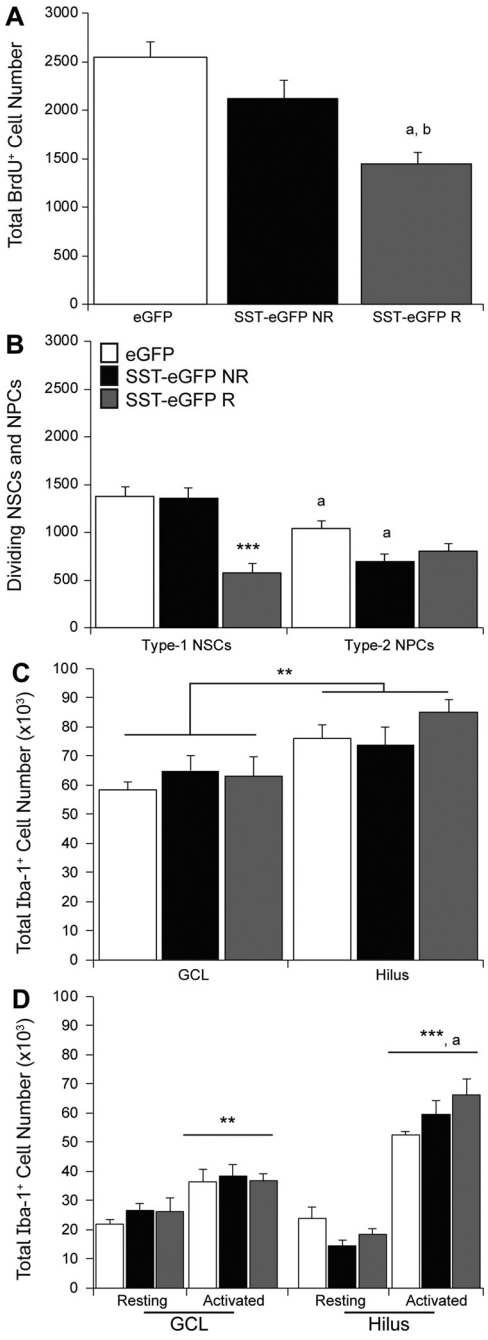

Fig. 6. Kindling-stimulated changes in Type-1 division were diminished in responders to SST gene transfer. (A) Stereological estimates of dividing BrdU$^+$ cell number revealed no difference between eGFP- and SST-eGFP vector-treated non-responders, but a significant decrease in SST-eGFP vector-treated responders versus eGFP vector-treated rats ($p < 0.01^a$) and SST-eGFP vector-treated non-responders ($p < 0.05^b$). **(B)** Quantification of the number of newly divided Type-1 NSCs and Type-2 NPCs revealed a decrease in the proliferation of BrdU$^+$ Type-1 NSCs in SST-eGFP vector-treated responders, but not in SST-eGFP vector-treated non-responders, versus eGFP vector-treated rats ($p < 0.001$***) and fewer BrdU$^+$ Type-2 NSCs in eGFP vector-treated ($p < 0.05^a$) and SST-eGFP vector-treated non-responders ($p < 0.001^a$) than BrdU$^+$ Type-1 NPCs, but not in SST-eGFP vector-treated responders. **(C)** Stereological estimates of Iba-1$^+$ microglia revealed no differences in microglia number between groups in either the GCL or hilus hippocampal subregions but more microglia in the hilus versus GCL of all groups combined ($p < 0.001$**). **(D)** Activated microglia outnumbered resting microglia in both the GCL ($p < 0.01$**) and hilus ($p < 0.001$***) and the number of activated microglia was higher in the hilus versus GCL ($p < 0.001^a$).

cells expressing each phenotype). Generally, more Type-1 NSCs were observed than Type-2 NPCs ($F_{(2,14)} = 20.54$; $p < 0.001$), but these numbers varied by group ($F_{(2,14)} = 7.45$; $p < 0.01$) and by the overall interaction ($F_{(2,14)} = 23.67$; $p < 0.0001$). Fewer dividing BrdU$^+$ cells were found in the dentate gyri of SST-eGFP responders versus eGFP vector-treated controls and SST-eGFP non-responders ($p < 0.01$ and $p < 0.05$, respectively). This effect was primarily due to the reduced number of dividing Type-1 NSCs found in the dentate gyri of SST-eGFP responders versus eGFP vector-treated controls and SST-eGFP non-responders (both p *values* < 0.001***). Moreover, fewer dividing Type-2 NPCs than dividing Type-1 NSCs were found in the dentate gyri of eGFP vector-treated controls ($p < 0.05^a$) and SST-eGFP non-responders ($p < 0.001^a$), but similar numbers of dividing Type-1 NSCs and Type-2 NPCs were observed in SST-eGFP-responders. These data suggest that sustained SST transgene expression may block the proliferation of Type-1 NSCs in behavioral responders.

Fig. 6**C** shows the mean (± S.E.M.) total number of microglia in the GCL and hilus of eGFP vector-treated controls, SST-eGFP non-responders, and SST-eGFP responders. More Iba-1$^+$ microglia were found in the hilus versus GCL ($F_{(2,14)} = 15.10$; $p < 0.01$), but the numbers neither varied by group ($F_{(2,14)} = 0.44$; $p = 0.66$) nor the overall interaction ($F_{(2,14)} = 1.09$; $p = 0.36$). Fig. 6**D** shows the mean (± S.E.M.) numbers of resting and activated Iba-1$^+$ microglia in the GCL and hilus of eGFP vector-treated controls, SST-eGFP non-responders and SST-eGFP responders (see Table 2 for percentages of Iba-1$^+$ cells expressing the activation marker CD11b). These numbers varied by region ($F_{(2,14)} = 15.10$; $p < 0.01$), activation state ($F_{(2,14)} = 207.97$; $p < 0.0001$) and the interaction between region and activation state ($F_{(1,6)} = 52.80$; $p < 0.0001$) but neither by group nor other interactions between the independent variables (all p *values* $\geq$ 0.09). Generally, hilar microglia outnumbered GCL microglia ($p < 0.01$) and activated microglia outnumbered resting microglia ($p < 0.001$). In fact, activated microglia outnumbered resting microglia in both the GCL ($p < 0.01$**) and hilus ($p < 0.001$***) and the number of activated microglia was higher in the hilus versus GCL ($p < 0.001^a$). The ratio of activated versus resting microglia was 1.54 in the GCL and the 2.89 in the hilus and the ratio of activated microglia in the hilus versus GCL was 1.54.

The total number of dividing Type-1 NSCs correlated positively with the total number of activated GCL ($r_{(17)} = 0.62$; $p < 0.0001$) and hilar ($r_{(17)} = 0.43$; $p < 0.05$) microglia and negatively with the total number of resting GCL ($r_{(17)} = -0.37$; $p < 0.05$) and hilar ($r_{(10)} = -0.44$; $p < 0.01$) microglia. These data suggest that microglial activation and Type-1 NSC proliferation may be related processes in the hippocampi of kindled rats.

4. Discussion

In this study, we tested whether sustained vector-mediated expression of a SST gene could alter the effects of kindling on neurogenesis and neuroinflammation in the dentate gyri of adult male rats. We found that the proliferation of Type-1 NSCs was stimulated in the hippocampi of kindled rats and observed a microglial response that persisted in the hilus for several weeks. These effects were also observed in the hippocampi of kindled rats that did not respond behaviorally to SST vector treatment. However, numbers of dividing Type-1 NSCs (but not activated microglia) were normalized in the hippocampi of rats that did respond behaviorally to SST vector treatment by exhibiting Grade 0 seizures on the test session. Our data are consistent with a role for aberrant neurogenesis in seizure maintenance and suggest the value of optimizing SST-based treatment strategies or alternatives that target upregulated Type-1 NSC division in models of temporal lobe epilepsy.

In agreement with studies employing single or repeated electrical stimulation protocols, we found that kindling upregulated the number of dividing cells in the hippocampi of adult rats (Bengzon et al., 1997; Nakagawa et al., 2000; Parent et al., 1998, 1997). Dividing cells in the hippocampal dentate gyrus can include relatively quiescent Type-1 NSCs with varied morphologies (Lugert et al., 2010) and more commonly proliferative, uncommitted Type-2a and neuronal lineage-committed Type -2b NPCs (Filippov et al., 2003; Kronenberg et al., 2003; Seri et al., 2001; Steiner et al., 2006; Suh et al., 2007). We add to the picture of how electrical kindling affects neurogenesis by showing that the number of dividing Type-1 NSCs (but not Type-2 NPCs) is elevated ˜3-fold even 48 h after rats experience their 3rd consecutive Grade 5 seizure in twice daily sessions or after rats that had already achieved criterion weeks earlier experience their final intermittent seizure in post-test sessions administered every 2–3 days. We expect that these increases may be more robust in this model at earlier time points (for example, 0–48 h) after the final seizure, as the neurogenic effect may degrade over time after an induced seizure (Nakagawa et al., 2000). Our finding is consistent with studies describing increased numbers of dividing Type-1 NSCs in the dentate gyri of rodents after electroconvulsive seizures or status epilepticus induced by the chemoconvulsants kainic acid and pilocarpine (Borges et al., 2006; Hüttmann et al., 2003; Segi-Nishida et al., 2008; Steiner et al., 2008; Zhu et al., 2005). Whether the abnormal upregulation of Type-1 NSC division in kindling models directly contributes to the production of ectopic granule neurons with aberrant morphologies and connectivity across epilepsy models is unclear.

The observation that supraphysiological numbers of new neurons with aberrant morphologies and connectivity are produced in the hippocampi of animals kindled electrically or chemically led to the hypothesis that aberrant neurogenesis may underlie seizure development and maintenance in epilepsy models (Jessberger and Parent, 2015). Several studies have shown that ablating neurogenesis with targeted γ-irradiation, anti-proliferative drug or genetic ablation strategies does not eliminate seizures but can reduce the number of seizures exhibited and their duration (Chen et al., 2001; Cho et al., 2015; Jung et al., 2004, 2006; Maesawa et al., 2000; Mori et al., 2000). Importantly, quiescent Type-1 NSCs are neither susceptible to these ablation strategies nor to doses of ^{3}[H]-thymidine or thymidine analogues that are lethal to dividing cells (Barazzuol et al., 2017; Cho et al., 2015; Morshead et al., 1994) rendering the ablation of neurogenesis using these strategies incomplete. Therefore, the development of novel strategies that specifically ablate quiescent Type-1 NSCs may be necessary to test the role that aberrant neurogenesis plays in the development and maintenance of seizures. Future work employing a complete ablation strategy would be necessary for testing whether SST vector-mediated changes in neurogenesis impacted seizure behavior or whether SST vector-mediated changes in seizure behavior impacted neurogenesis in SST-responder rats.

New neurons produced in the adult rodent hippocampus become morphologically and electrophysiologically indistinguishable from mature granule neurons after about a month (Cameron and McKay, 2001; Speisman et al., 2013a, b; van Praag et al., 1999a). Consistent with these data, we found that most 4 week-old cells expressed a mature neuronal phenotype in the dentate gyri of both sham-kindled and kindled rats. We did not specifically test whether new neurons matured and integrated more quickly in the dentate gyri of kindled versus sham-kindled rats (Overstreet-Wadiche et al., 2006), but we did observe similar ratios of dividing and surviving neurons between groups, suggesting that neuronal differentiation and the survival of new neurons was unaffected by the physiological changes that accompany the fully-kindled seizure susceptible state. Note that thymidine analogues are metabolically active for ˜2 h after injection, that NSCs/NPCs complete division in ˜ 24 h and divide several times and that a large number of progeny die within 2 weeks of birth in the adult hippocampus (Cameron and McKay, 2001; Cameron et al., 1993). The similar numbers of dividing cell numbers quantified 4 h after and surviving new neuron numbers quantified weeks after thymidine analogue injection in sham rats and in kindled rats in *Experiment 1* and in control vector and in SST-eGFP vector-treated rats in *Experiment 2* also supports the notion that

new neuron survival was not impacted by the seizure susceptible state, additional imposed seizures, vector injection or sustained SST or GFP expression. In fact, these results are consistent with other studies that quantify labeled cells in cage control animals at similar time points after a single thymidine analog injection (Cameron et al., 1993; Gould et al., 1999) and with the natural decline reported in surviving versus dividing numbers quantified at similar time points after multiple thymidine analog injections (Kempermann et al., 1997). Seizures can induce mossy fiber sprouting and ectopic migration in young neurons but more profoundly impact neurons born during or just after the seizure (Kron et al., 2010). Testing whether Type-1 NSCs that are stimulated to divide in the kindled brain produce Type-2a NPCs, Type-2b NPCs and/or neurons with more aberrant morphologies, placement or maturation rates than dividing Type-2 NPCs may provide insight into whether and how aberrant neurogenesis supports the development and maintenance of seizures.

Once fully kindled, rats continue to reliably produce robust evoked seizures across time and multiple tests (Brandt et al., 2004; Kalynchuk, 2000; Pinel and Rovner, 1978). Thus, any subsequent low-grade evoked seizure could be considered a response, whereas a prolonged reduction in evoked seizure grade may be considered therapeutic resilience. The key distinction lies in the question being asked. Our responder criterion based on evoked seizure grade upon the first re-stimulation after vector is clinically relevant and is often used in the preclinical study of antiepileptic drugs. An interesting aspect of the SST vector treatment was the all-or-none response, which we observed in prior work as well (Natarajan et al., 2017). Non-responder sub-populations are not unusual for antiepileptic therapies (Loscher, 2002; Loscher et al., 1993), and we took advantage of the varied responses to probe for any differences in neurogenesis and markers of inflammation between treatment responders versus non-responders.

Since SST vector blocked seizures in a subset of fully kindled rats and SST is anti-proliferative in other tissues, we hypothesized that SST may produce behavioral effects by modulating neurogenesis in the dentate gyri of kindled rats. We confirmed that sustained SST transgene expression blocks seizures in a subset of fully-kindled rats and normalized the division of Type-1 NSCs in dentate gyri of those rats. This effect is interesting because inhibitory hilar SSTergic neurons may selectively die early in epileptogenesis (Botterill et al., 2017; Buckmaster and Dudek, 1997; Robbins et al., 1991; Sloviter, 1987; Sun et al., 2007). It is possible that SST vector treatment indirectly mediates the reduction of Type-1 NSC division through its anti-epileptic effects, but our data raise the interesting possibility that vector-mediated SST expression may potentiate the anti-proliferative effects that surviving SSTergic neurons may exert on dividing Type-1 NSCs. Although SST expressing cells are found in the dentate gyrus SGZ/GCL region (Billova et al., 2007; Natarajan et al., 2017), whether NSCs and NPCs express SSTRs in adult animals is unknown. SST does modulate neuronal migration during embryogenesis and embryonic NSCs/NPCs express SSTRs (Maubert et al., 1994; Yacubova and Komuro, 2002). In addition, $SSTR_2$ agonists suppress the adrenalectomy-induced proliferation of pituitary cells and TGF-β works through SST to suppress the expansion of neuroendocrine tumor cells (Leu et al., 2008; Nolan et al., 2007). Future experiments that identify the mechanisms through which SST modulates Type-1 NSC proliferation may lead to better SST responder rates, since SSTR expression could differ between SST responder and non-responder rats. Our earlier work demonstrated a higher responder rate when vector-mediated SST expression was initiated before the onset of kindling sessions (Zafar et al., 2012), suggesting that SST may work through transient mechanisms with timing that varied between responder and non-responder rats. After a certain period of time hypothesized changes that underlie seizure development and maintenance may become more permanent and difficult to reverse. For instance, earlier treatment may largely prevent the maturation of networks composed of high numbers of seizure-induced, new neurons with aberrant morphologies and connectivity (Botterill et al., 2015; Parent et al., 2006). We have observed increased staining for somatostatin in SST-eGFP treated rats (Natarajan et al., 2017), but it is difficult to confirm increased release of the neuropeptide from transfected neurons and whether that varied between responders and non-responders. In the same vein, although we detected similar infection intensities and overall SST responder rates between *Experiment 2*, which employed a SST-eGFP vector with a medium titer (1.0×10^{13} vg/ml; 2/4 responders) and *Experiment 3*, which employed SST-eGFP vectors with lower (6.1×10^{12} vg/ml; 1/7 responders) or higher (4.9×10^{13} vg/ml; 4/6 responders) titers, SST responder ratios suggest that responder rates may increase with increasing titers. However, differences in design between *Experiments 2* and *3* and low rat numbers within each titer group precluded direct comparison of the effects of titer dose on dividing Type-1 NSCs and on seizure severity. Future work should experimentally test whether SST vector titer dose impacts these variables.

While neuroinflammation is typically reported to compromise neurogenesis (Chen et al., 2011; Ekdahl et al., 2003; Lee et al., 2013; Monje et al., 2003; Ormerod et al., 2013), neurogenesis and neuroinflammation are both potentiated in the hippocampi of kindled rats (Bengzon et al., 1997; Khurgel and Ivy, 1996; Parent et al., 1998, 1997; Plata-Salamán et al., 2000). In the current study, we found an increased number of activated microglia immediately after rats exhibited their 3rd Grade 5 seizure that persisted most robustly in the hilus for at least 4 weeks. The increased number of dividing Type-1 NSCs found in the dentate gyri of kindled rats after they exhibited their 3rd Grade 5 seizure both correlated positively with activated microglia number and translated into a similar increase in new neuron number 4 weeks later. Given that complex stimuli can produce variable microglial activation states (Butovsky et al., 2006; Siddiqui et al., 2016), kindling could stimulate a microglial activation state that differs from that which ablates neurogenesis in other models. For instance, seizures can induce the microglial production of insulin-like growth factor-1, which stimulates hippocampal cell proliferation (Aberg et al., 2003; Beck et al., 1995; Choi et al., 2008; O'Kusky et al., 2000; Trejo et al., 2001) and reducing microglial activation after status epilepticus by blocking microglial $CX3CR_1$ signaling normalizes subgranular zone cell proliferation (Ali et al., 2015). We are currently profiling hippocampal protein samples of control, kindled and vector-treated kindled rats to identify which cytokines vary in concentration across these contexts. Alternatively, kindling may produce a neuroinflammatory response similar to that which ablates neurogenesis that is initially superseded by another physiological effect produced by kindling and/or kindled seizures. The observation that hippocampal neurogenesis is severely diminished in chronic epilepsy models or in individuals with chronic epilepsy (D'Alessio et al., 2010; Hattiangady et al., 2004) suggests that either the chronic neuroinflammatory response eventually compromises neurogenesis or possibly that the progenitor pool becomes exhausted by the initial supraphysiological upregulation of Type-1 NSC division. Identifying the mechanisms through which neurogenesis is modulated in the kindled brain may provide insights into novel therapeutic strategies.

5. Conclusions

We demonstrated that the number of dividing Type-1 NSCs is potently increased 48 h after kindled rats exhibit their 3rd consecutive Grade 5 seizure and that, within a subset of rats that respond behaviorally to sustained vector-mediated SST expression, this number is normalized. This finding encourages the refinement of strategies that more specifically target SST signaling and their timing with the intention of improving response rates in future work. Consistent with previous work, the increase in dividing Type-1 NSCs that we observed was paradoxically associated with an increase in the number of activated microglia in the GCL and a more robust and persistent increase in the hilus of kindled rats and this neuroinflammatory response was unaffected by vector treatment. Testing whether or how the neuroinflammatory or other physiological responses that accompany epilepsy

or that are stimulated by kindling in animal models of epilepsy may uniquely render neurogenesis aberrant may provide insight into the mechanisms that drive the development and maintenance of seizure behavior. Collectively, our results support the hypothesis that Type-1 NSCs may be a novel target for epilepsy treatments and that aberrant neurogenesis *could be* a cellular mechanism of seizure development and maintenance. Of course, future work employing complete neurogenesis ablation strategies (i.e. targeting resistant Type-1 NSCs) would be required to test whether aberrant neurogenesis (through the upregulation of Type-1 NSCs) is a cellular mechanism for epilepsy or physiological response to seizures. In the latter case, aberrantly connected young neurons could still provide a cellular substrate for seizure maintenance.

Acknowledgements

We thank Haley Bross, Nicholas Gregory and James McGuiness for technical support, Dr. Malcolm Maden for valuable comments regarding the manuscript and Dr. Michael King for technical support and his comments regarding the manuscript. This research was supported by the Department of Defense Congressionally Directed Medical Research Programs (CDMRP) Grant Number PR121769, the Wilder Center of Excellence for Epilepsy Research, the Children's Miracle Network and NIH Grant #R03 AGO49411. This work was also supported by resources provided by the College of Engineering at the University of Florida. The contents do not represent the views of the U.S Department of veterans Affairs or the United States Government.

References

Aberg, M.A., Aberg, N.D., Palmer, T.D., Alborn, A.M., Carlsson-Skwirut, C., Bang, P., Rosengren, L.E., Olsson, T., Gage, F.H., Eriksson, P.S., 2003. IGF-I has a direct proliferative effect in adult hippocampal progenitor cells. Mol. Cell. Neurosci. 24, 23–40.

Aimone, J.B., Li, Y., Lee, S.W., Clemenson, G.D., Deng, W., Gage, F.H., 2014. Regulation and function of adult neurogenesis: from genes to cognition. Physiol. Rev. 94, 991–1026.

Ali, I., Chugh, D., Ekdahl, C.T., 2015. Role of fractalkine-CX3CR1 pathway in seizure-induced microglial activation, neurodegeneration, and neuroblast production in the adult rat brain. Neurobiol. Dis. 74, 194–203.

Altman, J., 1962. Are new neurons formed in the brains of adult mammals? Science 135, 1127–1128.

Aourz, N., De Bundel, D., Stragier, B., Clinckers, R., Portelli, J., Michotte, Y., Smolders, I., 2011. Rat hippocampal somatostatin sst3 and sst4 receptors mediate anticonvulsive effects in vivo: indications of functional interactions with sst2 receptors. Neuropharmacology 61, 1327–1333.

Bañuelos, C., LaSarge, C.L., McQuail, J.A., Hartman, J.J., Gilbert, R.J., Ormerod, B.K., Bizon, J.L., 2013. Age-related changes in rostral basal forebrain cholinergic and GABAergic projection neurons: relationship with spatial impairment. Neurobiol. Aging 34, 845–862.

Baratta, M.V., Lamp, T., Tallent, M.K., 2002. Somatostatin depresses long-term potentiation and Ca2+ signaling in mouse dentate gyrus. J. Neurophysiol. 88, 3078–3086.

Barazzuol, L., Ju, L., Jeggo, P.A., 2017. A coordinated DNA damage response promotes adult quiescent neural stem cell activation. PLoS Biol. 15, e2001264.

Beck, K.D., Powell-Braxton, L., Widmer, H.R., Valverde, J., Hefti, F., 1995. Igf1 gene disruption results in reduced brain size, CNS hypomyelination, and loss of hippocampal granule and striatal parvalbumin-containing neurons. Neuron 14, 717–730.

Bengzon, J., Kokaia, Z., Elmér, E., Nanobashvili, A., Kokaia, M., Lindvall, O., 1997. Apoptosis and proliferation of dentate gyrus neurons after single and intermittent limbic seizures. Proc. Natl. Acad. Sci. U. S. A. 94, 10432–10437.

Bezchlibnyk, Y.B., Sun, X., Wang, J.F., MacQueen, G.M., McEwen, B.S., Young, L.T., 2007. Neuron somal size is decreased in the lateral amygdalar nucleus of subjects with bipolar disorder. J. Psychiatry Neurosci. 32, 203–210.

Billova, S., Galanopoulou, A.S., Seidah, N.G., Qiu, X., Kumar, U., 2007. Immunohistochemical expression and colocalization of somatostatin, carboxypeptidase-E and prohormone convertases 1 and 2 in rat brain. Neuroscience 147, 403–418.

Borges, K., McDermott, D., Irier, H., Smith, Y., Dingledine, R., 2006. Degeneration and proliferation of astrocytes in the mouse dentate gyrus after pilocarpine-induced status epilepticus. Exp. Neurol. 201, 416–427.

Botterill, J.J., Brymer, K.J., Caruncho, H.J., Kalynchuk, L.E., 2015. Aberrant hippocampal neurogenesis after limbic kindling: relationship to BDNF and hippocampal-dependent memory. Epilepsy Behav. 47, 83–92.

Botterill, J.J., Nogovitsyn, N., Caruncho, H.J., Kalynchuk, L.E., 2017. Selective plasticity of hippocampal GABAergic interneuron populations following kindling of different brain regions. J. Comp. Neurol. 525, 389–406.

Boyce, R.W., Dorph-Petersen, K.A., Lyck, L., Gundersen, H.J., 2010. Design-based stereology: introduction to basic concepts and practical approaches for estimation of cell number. Toxicol. Pathol. 38, 1011–1025.

Brandt, C., Ebert, U., Loscher, W., 2004. Epilepsy induced by extended amygdala-kindling in rats: lack of clear association between development of spontaneous seizures and neuronal damage. Epilepsy Res. 62, 135–156.

Buckmaster, P.S., Dudek, F.E., 1997. Neuron loss, granule cell axon reorganization, and functional changes in the dentate gyrus of epileptic kainate-treated rats. J. Comp. Neurol. 385, 385–404.

Buckmaster, P.S., Otero-Corchón, V., Rubinstein, M., Low, M.J., 2002. Heightened seizure severity in somatostatin knockout mice. Epilepsy Res. 48, 43–56.

Burns, K.A., Kuan, C.Y., 2005. Low doses of bromo- and iododeoxyuridine produce near-saturation labeling of adult proliferative populations in the dentate gyrus. Eur. J. Neurosci. 21, 803–807.

Butovsky, O., Ziv, Y., Schwartz, A., Landa, G., Talpalar, A.E., Pluchino, S., Martino, G., Schwartz, M., 2006. Microglia activated by IL-4 or IFN-gamma differentially induce neurogenesis and oligodendrogenesis from adult stem/progenitor cells. Mol. Cell. Neurosci. 31, 149–160.

Cameron, H.A., McKay, R.D., 2001. Adult neurogenesis produces a large pool of new granule cells in the dentate gyrus. J. Comp. Neurol. 435, 406–417.

Cameron, H.A., Woolley, C.S., McEwen, B.S., Gould, E., 1993. Differentiation of newly born neurons and glia in the dentate gyrus of the adult rat. Neuroscience 56, 337–344.

Chen, Z.F., Kamiryo, T., Henson, S.L., Yamamoto, H., Bertram, E.H., Schottler, F., Patel, F., Steiner, L., Prasad, D., Kassell, N.F., Shareghis, S., Lee, K.S., 2001. Anticonvulsant effects of gamma surgery in a model of chronic spontaneous limbic epilepsy in rats. J. Neurosurg. 94, 270–280.

Chen, Z., Phillips, L.K., Gould, E., Campisi, J., Lee, S.W., Ormerod, B.K., Zwierzchoniewska, M., Martinez, O.M., Palmer, T.D., 2011. MHC mismatch inhibits neurogenesis and neuron maturation in stem cell allografts. PLoS One 6, e14787.

Cho, K.O., Lybrand, Z.R., Ito, N., Brulet, R., Tafacory, F., Zhang, L., Good, L., Ure, K., Kernie, S.G., Birnbaum, S.G., Scharfman, H.E., Eisch, A.J., Hsieh, J., 2015. Aberrant hippocampal neurogenesis contributes to epilepsy and associated cognitive decline. Nat. Commun. 6, 6606.

Choi, Y.S., Cho, H.Y., Hoyt, K.R., Naegele, J.R., Obrietan, K., 2008. IGF-1 receptor-mediated ERK/MAPK signaling couples status epilepticus to progenitor cell proliferation in the subgranular layer of the dentate gyrus. Glia 56, 791–800.

Cliff, N., 1993. Dominance statistics: ordinal analyses to answer ordinal questions. Psychol. Bull. 114, 494–509.

Csaba, Z., Dournaud, P., 2001. Cellular biology of somatostatin receptors. Neuropeptides 35, 1–23.

D'Alessio, L., Konopka, H., López, E.M., Seoane, E., Consalvo, D., Oddo, S., Kochen, S., López-Costa, J.J., 2010. Doublecortin (DCX) immunoreactivity in hippocampus of chronic refractory temporal lobe epilepsy patients with hippocampal sclerosis. Seizure 19, 567–572.

Dun, S.L., Brailoiu, G.C., Tica, A.A., Yang, J., Chang, J.K., Brailoiu, E., Dun, N.J., 2010. Neuronostatin is co-expressed with somatostatin and mobilizes calcium in cultured rat hypothalamic neurons. Neuroscience 166, 455–463.

Ekdahl, C.T., Claasen, J.H., Bonde, S., Kokaia, Z., Lindvall, O., 2003. Inflammation is detrimental for neurogenesis in adult brain. Proc. Natl. Acad. Sci. U. S. A. 100, 13632–13637.

Eriksson, P.S., Perfilieva, E., Björk-Eriksson, T., Alborn, A.M., Nordborg, C., Peterson, D.A., Gage, F.H., 1998. Neurogenesis in the adult human hippocampus. Nat. Med. 4, 1313–1317.

Filippov, V., Kronenberg, G., Pivneva, T., Reuter, K., Steiner, B., Wang, L.P., Yamaguchi, M., Kettenmann, H., Kempermann, G., 2003. Subpopulation of nestin-expressing progenitor cells in the adult murine hippocampus shows electrophysiological and morphological characteristics of astrocytes. Mol. Cell. Neurosci. 23, 373–382.

Fournier, N.M., Andersen, D.R., Botterill, J.J., Sterner, E.Y., Lussier, A.L., Caruncho, H.J., Kalynchuk, L.E., 2010. The effect of amygdala kindling on hippocampal neurogenesis coincides with decreased reelin and DISC1 expression in the adult dentate gyrus. Hippocampus 20, 659–671.

Fournier, N.M., Botterill, J.J., Marks, W.N., Guskjolen, A.J., Kalynchuk, L.E., 2013. Impaired recruitment of seizure-generated neurons into functional memory networks of the adult dentate gyrus following long-term amygdala kindling. Exp. Neurol. 244, 96–104.

Freund, T.F., Buzsáki, G., 1996. Interneurons of the hippocampus. Hippocampus 6, 347–470.

Gonçalves, J.T., Schafer, S.T., Gage, F.H., 2016. Adult neurogenesis in the hippocampus: from stem cells to behavior. Cell 167, 897–914.

Gould, E., Beylin, A., Tanapat, P., Reeves, A., Shors, T.J., 1999. Learning enhances adult neurogenesis in the hippocampal formation. Nat. Neurosci. 2, 260–265.

Hattiangady, B., Rao, M.S., Shetty, A.K., 2004. Chronic temporal lobe epilepsy is associated with severely declined dentate neurogenesis in the adult hippocampus. Neurobiol. Dis. 17, 473–490.

Hüttmann, K., Sadgrove, M., Wallraff, A., Hinterkeuser, S., Kirchhoff, F., Steinhäuser, C., Gray, W.P., 2003. Seizures preferentially stimulate proliferation of radial glia-like astrocytes in the adult dentate gyrus: functional and immunocytochemical analysis. Eur. J. Neurosci. 18, 2769–2778.

Jessberger, S., Parent, J.M., 2015. Epilepsy and adult neurogenesis. Cold Spring Harb. Perspect. Biol. 7.

Jessberger, S., Nakashima, K., Clemenson, G.D., Mejia, E., Mathews, E., Ure, K., Ogawa, S., Sinton, C.M., Gage, F.H., Hsieh, J., 2007a. Epigenetic modulation of seizure-induced neurogenesis and cognitive decline. J. Neurosci. 27, 5967–5975.

Jessberger, S., Zhao, C., Toni, N., Clemenson, G.D., Li, Y., Gage, F.H., 2007b. Seizure-associated, aberrant neurogenesis in adult rats characterized with retrovirus-mediated cell labeling. J. Neurosci. 27, 9400–9407.

Jung, K.H., Chu, K., Kim, M., Jeong, S.W., Song, Y.M., Lee, S.T., Kim, J.Y., Lee, S.K., Roh,

J.K., 2004. Continuous cytosine-b-D-arabinofuranoside infusion reduces ectopic granule cells in adult rat hippocampus with attenuation of spontaneous recurrent seizures following pilocarpine-induced status epilepticus. Eur. J. Neurosci. 19, 3219–3226.
Jung, K.H., Chu, K., Lee, S.T., Kim, J., Sinn, D.I., Kim, J.M., Park, D.K., Lee, J.J., Kim, S.U., Kim, M., Lee, S.K., Roh, J.K., 2006. Cyclooxygenase-2 inhibitor, celecoxib, inhibits the altered hippocampal neurogenesis with attenuation of spontaneous recurrent seizures following pilocarpine-induced status epilepticus. Neurobiol. Dis. 23, 237–246.
Kalynchuk, L.E., 2000. Long-term amygdala kindling in rats as a model for the study of interictal emotionality in temporal lobe epilepsy. Neurosci. Biobehav. Rev. 24, 691–704.
Kapur, J., 2013. Somatostatin type-2 receptor activation inhibits glutamate release and prevents status epilepticus. Neurobiol. Dis. 54, 94–104.
Kempermann, G., Kuhn, H.G., Gage, F.H., 1997. Genetic influence on neurogenesis in the dentate gyrus of adult mice. Proc. Natl. Acad. Sci. U. S. A. 94, 10409–10414.
Kempermann, G., Jessberger, S., Steiner, B., Kronenberg, G., 2004. Milestones of neuronal development in the adult hippocampus. Trends Neurosci. 27, 447–452.
Khurgel, M., Ivy, G.O., 1996. Astrocytes in kindling: relevance to epileptogenesis. Epilepsy Res. 26, 163–175.
Kron, M.M., Zhang, H., Parent, J.M., 2010. The developmental stage of dentate granule cells dictates their contribution to seizure-induced plasticity. J. Neurosci. 30, 2051–2059.
Kronenberg, G., Reuter, K., Steiner, B., Brandt, M.D., Jessberger, S., Yamaguchi, M., Kempermann, G., 2003. Subpopulations of proliferating cells of the adult hippocampus respond differently to physiologic neurogenic stimuli. J. Comp. Neurol. 467, 455–463.
Larsen, J.O., 1998. Stereology of nerve cross sections. J. Neurosci. Methods 85, 107–118.
Lee, S.W., Haditsch, U., Cord, B.J., Guzman, R., Kim, S.J., Boettcher, C., Priller, J., Ormerod, B.K., Palmer, T.D., 2013. Absence of CCL2 is sufficient to restore hippocampal neurogenesis following cranial irradiation. Brain Behav. Immun. 30, 33–44.
Leu, F.P., Nandi, M., Niu, C., 2008. The effect of transforming growth factor beta on human neuroendocrine tumor BON cell proliferation and differentiation is mediated through somatostatin signaling. Mol. Cancer Res. 6, 1029–1042.
Loscher, W., 2002. Animal models of drug-resistant epilepsy. Novartis Found. Symp. 243, 149–159 discussion 159-166, 180-145.
Loscher, W., Rundfeldt, C., Honack, D., 1993. Pharmacological characterization of phenytoin-resistant amygdala-kindled rats, a new model of drug-resistant partial epilepsy. Epilepsy Res. 15, 207–219.
Lugert, S., Basak, O., Knuckles, P., Haussler, U., Fabel, K., Gotz, M., Haas, C.A., Kempermann, G., Taylor, V., Giachino, C., 2010. Quiescent and active hippocampal neural stem cells with distinct morphologies respond selectively to physiological and pathological stimuli and aging. Cell Stem Cell 6, 445–456.
Maesawa, S., Kondziolka, D., Dixon, C.E., Balzer, J., Fellows, W., Lunsford, L.D., 2000. Subnecrotic stereotactic radiosurgery controlling epilepsy produced by kainic acid injection in rats. J. Neurosurg. 93, 1033–1040.
Maubert, E., Slama, A., Ciofi, P., Viollet, C., Tramu, G., Dupouy, J.P., Epelbaum, J., 1994. Developmental patterns of somatostatin-receptors and somatostatin-immunoreactivity during early neurogenesis in the rat. Neuroscience 62, 317–325.
Monje, M.L., Mizumatsu, S., Fike, J.R., Palmer, T.D., 2002. Irradiation induces neural precursor-cell dysfunction. Nat. Med. 8, 955–962.
Monje, M.L., Toda, H., Palmer, T.D., 2003. Inflammatory blockade restores adult hippocampal neurogenesis. Science 302, 1760–1765.
Monno, A., Rizzi, M., Samanin, R., Vezzani, A., 1993. Anti-somatostatin antibody enhances the rate of hippocampal kindling in rats. Brain Res. 602, 148–152.
Mori, Y., Kondziolka, D., Balzer, J., Fellows, W., Flickinger, J.C., Lunsford, L.D., Thulborn, K.R., 2000. Effects of stereotactic radiosurgery on an animal model of hippocampal epilepsy. Neurosurgery 46, 157–165 discussion 165-158.
Morshead, C.M., Reynolds, B.A., Craig, C.G., McBurney, M.W., Staines, W.A., Morassutti, D., Weiss, S., van der Kooy, D., 1994. Neural stem cells in the adult mammalian forebrain: a relatively quiescent subpopulation of subependymal cells. Neuron 13, 1071–1082.
Nakagawa, E., Aimi, Y., Yasuhara, O., Tooyama, I., Shimada, M., McGeer, P.L., Kimura, H., 2000. Enhancement of progenitor cell division in the dentate gyrus triggered by initial limbic seizures in rat models of epilepsy. Epilepsia 41, 10–18.
Natarajan, G., Leibowitz, J.A., Zhou, J., Zhao, Y., McElroy, J.A., King, M.A., Ormerod, B.K., Carney, P.R., 2017. Adeno-associated viral vector-mediated preprosomatostatin expression suppresses induced seizures in kindled rats. Epilepsy Res. 130, 81–92.
Nickell, C.R.G., Peng, H., Hayes, D.M., Chen, K.Y., McClain, J.A., Nixon, K., 2017. Type 2 neural progenitor cell activation drives reactive neurogenesis after binge-like alcohol exposure in adolescent male rats. Front. Psychiatry 8, 283.
Nolan, L.A., Schmid, H.A., Levy, A., 2007. Octreotide and the novel multireceptor ligand somatostatin receptor agonist pasireotide (SOM230) block the adrenalectomy-induced increase in mitotic activity in male rat anterior pituitary. Endocrinology 148, 2821–2827.
Noori, H.R., Fornal, C.A., 2011. The appropriateness of unbiased optical fractionators to assess cell proliferation in the adult hippocampus. Front. Neurosci. 5, 140.
O'Kusky, J.R., Ye, P., D'Ercole, A.J., 2000. Insulin-like growth factor-I promotes neurogenesis and synaptogenesis in the hippocampal dentate gyrus during postnatal development. J. Neurosci. 20, 8435–8442.
Olias, G., Viollet, C., Kusserow, H., Epelbaum, J., Meyerhof, W., 2004. Regulation and function of somatostatin receptors. J. Neurochem. 89, 1057–1091.
Olson, A.K., Eadie, B.D., Ernst, C., Christie, B.R., 2006. Environmental enrichment and voluntary exercise massively increase neurogenesis in the adult hippocampus via dissociable pathways. Hippocampus 16, 250–260.
Ormerod, B.K., Hanft, S.J., Asokan, A., Haditsch, U., Lee, S.W., Palmer, T.D., 2013. PPARγ activation prevents impairments in spatial memory and neurogenesis following transient illness. Brain Behav. Immun. 29, 28–38.
Overstreet-Wadiche, L.S., Bromberg, D.A., Bensen, A.L., Westbrook, G.L., 2006. Seizures accelerate functional integration of adult-generated granule cells. J. Neurosci. 26, 4095–4103.
Parent, J.M., Yu, T.W., Leibowitz, R.T., Geschwind, D.H., Sloviter, R.S., Lowenstein, D.H., 1997. Dentate granule cell neurogenesis is increased by seizures and contributes to aberrant network reorganization in the adult rat hippocampus. J. Neurosci. 17, 3727–3738.
Parent, J.M., Janumpalli, S., McNamara, J.O., Lowenstein, D.H., 1998. Increased dentate granule cell neurogenesis following amygdala kindling in the adult rat. Neurosci. Lett. 247, 9–12.
Parent, J.M., Tada, E., Fike, J.R., Lowenstein, D.H., 1999. Inhibition of dentate granule cell neurogenesis with brain irradiation does not prevent seizure-induced mossy fiber synaptic reorganization in the rat. J. Neurosci. 19, 4508–4519.
Parent, J.M., Elliott, R.C., Pleasure, S.J., Barbaro, N.M., Lowenstein, D.H., 2006. Aberrant seizure-induced neurogenesis in experimental temporal lobe epilepsy. Ann. Neurol. 59, 81–91.
Paxinos, G., Watson, C., 2007. The Rat Brain in Stereotaxic Coordinates, sixth ed. Elsevier, Amsterdam.
Pekcec, A., Potschka, H., 2007. Newborn neurons with hilar basal dendrites hallmark epileptogenic networks. Neuroreport 18, 585–589.
Pekcec, A., Fuest, C., Mühlenhoff, M., Gerardy-Schahn, R., Potschka, H., 2008. Targeting epileptogenesis-associated induction of neurogenesis by enzymatic depolysialylation of NCAM counteracts spatial learning dysfunction but fails to impact epilepsy development. J. Neurochem. 105, 389–400.
Pinel, J.P., Rovner, L.I., 1978. Experimental epileptogenesis: kindling-induced epilepsy in rats. Exp. Neurol. 58, 190–202.
Plata-Salamán, C.R., Ilyin, S.E., Turrin, N.P., Gayle, D., Flynn, M.C., Romanovitch, A.E., Kelly, M.E., Bureau, Y., Anisman, H., McIntyre, D.C., 2000. Kindling modulates the IL-1beta system, TNF-alpha, TGF-beta1, and neuropeptide mRNAs in specific brain regions. Brain Res. Mol. Brain Res. 75, 248–258.
Pun, R.Y., Rolle, I.J., Lasarge, C.L., Hosford, B.E., Rosen, J.M., Uhl, J.D., Schmeltzer, S.N., Faulkner, C., Bronson, S.L., Murphy, B.L., Richards, D.A., Holland, K.D., Danzer, S.C., 2012. Excessive activation of mTOR in postnatally generated granule cells is sufficient to cause epilepsy. Neuron 75, 1022–1034.
Qiu, C., Zeyda, T., Johnson, B., Hochgeschwender, U., de Lecea, L., Tallent, M.K., 2008. Somatostatin receptor subtype 4 couples to the M-current to regulate seizures. J. Neurosci. 28, 3567–3576.
Racine, R.J., 1972. Modification of seizure activity by electrical stimulation. I. After-discharge threshold. Electroencephalogr. Clin. Neurophysiol. 32, 269–279.
Racine, R.J., Gartner, J.G., Burnham, W.M., 1972. Epileptiform activity and neural plasticity in limbic structures. Brain Res. 47, 262–268.
Reisine, T., Bell, G.I., 1995. Molecular biology of somatostatin receptors. Endocr. Rev. 16, 427–442.
Robbins, R.J., Brines, M.L., Kim, J.H., Adrian, T., de Lanerolle, N., Welsh, S., Spencer, D.D., 1991. A selective loss of somatostatin in the hippocampus of patients with temporal lobe epilepsy. Ann. Neurol. 29, 325–332.
Samson, W.K., Zhang, J.V., Avsian-Kretchmer, O., Cui, K., Yosten, G.L., Klein, C., Lyu, R.M., Wang, Y.X., Chen, X.Q., Yang, J., Price, C.J., Hoyda, T.D., Ferguson, A.V., Yuan, X.B., Chang, J.K., Hsueh, A.J., 2008. Neuronostatin encoded by the somatostatin gene regulates neuronal, cardiovascular, and metabolic functions. J. Biol. Chem. 283, 31949–31959.
Samson, W.K., Stein, L.M., Elrick, M., Salvatori, A., Kolar, G., Corbett, J.A., Yosten, G.L., 2016. Hypoglycemia unawareness prevention: targeting glucagon production. Physiol. Behav. 162, 147–150.
Scharfman, H.E., Hen, R., 2007. Neuroscience. Is more neurogenesis always better? Science 315, 336–338.
Scharfman, H.E., Goodman, J.H., Sollas, A.L., Croll, S.D., 2002. Spontaneous limbic seizures after intrahippocampal infusion of brain-derived neurotrophic factor. Exp. Neurol. 174, 201–214.
Scharfman, H., Goodman, J., Macleod, A., Phani, S., Antonelli, C., Croll, S., 2005. Increased neurogenesis and the ectopic granule cells after intrahippocampal BDNF infusion in adult rats. Exp. Neurol. 192, 348–356.
Schindler, M., Humphrey, P.P., Emson, P.C., 1996. Somatostatin receptors in the central nervous system. Prog. Neurobiol. 50, 9–47.
Schindler, M., Sellers, L.A., Humphrey, P.P., Emson, P.C., 1997. Immunohistochemical localization of the somatostatin SST2(A) receptor in the rat brain and spinal cord. Neuroscience 76, 225–240.
Schulz, S., Handel, M., Schreff, M., Schmidt, H., Hollt, V., 2000. Localization of five somatostatin receptors in the rat central nervous system using subtype-specific antibodies. J. Physiol. Paris 94, 259–264.
Segi-Nishida, E., Warner-Schmidt, J.L., Duman, R.S., 2008. Electroconvulsive seizure and VEGF increase the proliferation of neural stem-like cells in rat hippocampus. Proc. Natl. Acad. Sci. U. S. A. 105, 11352–11357.
Seri, B., García-Verdugo, J.M., McEwen, B.S., Alvarez-Buylla, A., 2001. Astrocytes give rise to new neurons in the adult mammalian hippocampus. J. Neurosci. 21, 7153–7160.
Siddiqui, T.A., Lively, S., Schlichter, L.C., 2016. Complex molecular and functional outcomes of single versus sequential cytokine stimulation of rat microglia. J. Neuroinflammation 13, 66.
Sloviter, R.S., 1987. Decreased hippocampal inhibition and a selective loss of interneurons in experimental epilepsy. Science 235, 73–76.
Speisman, R.B., Kumar, A., Rani, A., Foster, T.C., Ormerod, B.K., 2013a. Daily exercise improves memory, stimulates hippocampal neurogenesis and modulates immune and neuroimmune cytokines in aging rats. Brain Behav. Immun. 28, 25–43.

Speisman, R.B., Kumar, A., Rani, A., Pastoriza, J.M., Severance, J.E., Foster, T.C., Ormerod, B.K., 2013b. Environmental enrichment restores neurogenesis and rapid acquisition in aged rats. Neurobiol. Aging 34, 263–274.
Steiner, B., Klempin, F., Wang, L., Kott, M., Kettenmann, H., Kempermann, G., 2006. Type-2 cells as link between glial and neuronal lineage in adult hippocampal neurogenesis. Glia 54, 805–814.
Steiner, B., Zurborg, S., Hörster, H., Fabel, K., Kempermann, G., 2008. Differential 24 h responsiveness of Prox1-expressing precursor cells in adult hippocampal neurogenesis to physical activity, environmental enrichment, and kainic acid-induced seizures. Neuroscience 154, 521–529.
Suh, H., Consiglio, A., Ray, J., Sawai, T., D'Amour, K.A., Gage, F.H., 2007. In vivo fate analysis reveals the multipotent and self-renewal capacities of Sox2+ neural stem cells in the adult hippocampus. Cell Stem Cell 1, 515–528.
Sun, C., Mtchedlishvili, Z., Bertram, E.H., Erisir, A., Kapur, J., 2007. Selective loss of dentate hilar interneurons contributes to reduced synaptic inhibition of granule cells in an electrical stimulation-based animal model of temporal lobe epilepsy. J. Comp. Neurol. 500, 876–893.
Tallent, M.K., Siggins, G.R., 1997. Somatostatin depresses excitatory but not inhibitory neurotransmission in rat CA1 hippocampus. J. Neurophysiol. 78, 3008–3018.
Trejo, J.L., Carro, E., Torres-Aleman, I., 2001. Circulating insulin-like growth factor I mediates exercise-induced increases in the number of new neurons in the adult hippocampus. J. Neurosci. 21, 1628–1634.
van Praag, H., Christie, B.R., Sejnowski, T.J., Gage, F.H., 1999a. Running enhances neurogenesis, learning, and long-term potentiation in mice. Proc. Natl. Acad. Sci. U. S. A. 96, 13427–13431.
van Praag, H., Kempermann, G., Gage, F.H., 1999b. Running increases cell proliferation and neurogenesis in the adult mouse dentate gyrus. Nat. Neurosci. 2, 266–270.
van Praag, H., Schinder, A.F., Christie, B.R., Toni, N., Palmer, T.D., Gage, F.H., 2002. Functional neurogenesis in the adult hippocampus. Nature 415, 1030–1034.
van Praag, H., Shubert, T., Zhao, C., Gage, F.H., 2005. Exercise enhances learning and hippocampal neurogenesis in aged mice. J. Neurosci. 25, 8680–8685.
Vezzani, A., Serafini, R., Stasi, M.A., Viganò, G., Rizzi, M., Samanin, R., 1991. A peptidase-resistant cyclic octapeptide analogue of somatostatin (SMS 201-995) modulates seizures induced by quinolinic and kainic acids differently in the rat hippocampus. Neuropharmacology 30, 345–352.
Viollet, C., Lepousez, G., Loudes, C., Videau, C., Simon, A., Epelbaum, J., 2008. Somatostatinergic systems in brain: networks and functions. Mol. Cell. Endocrinol. 286, 75–87.
West, M.J., Slomianka, L., Gundersen, H.J., 1991. Unbiased stereological estimation of the total number of neurons in thesubdivisions of the rat hippocampus using the optical fractionator. Anat. Rec. 231, 482–497.
Yacubova, E., Komuro, H., 2002. Stage-specific control of neuronal migration by somatostatin. Nature 415, 77–81.
Zafar, R., King, M.A., Carney, P.R., 2012. Adeno associated viral vector-mediated expression of somatostatin in rat hippocampus suppresses seizure development. Neurosci. Lett. 509, 87–91.
Zeng, C., Pan, F., Jones, L.A., Lim, M.M., Griffin, E.A., Sheline, Y.I., Mintun, M.A., Holtzman, D.M., Mach, R.H., 2010. Evaluation of 5-ethynyl-2'-deoxyuridine staining as a sensitive and reliable method for studying cell proliferation in the adult nervous system. Brain Res. 1319, 21–32.
Zhu, H., Dahlström, A., Hansson, H.A., 2005. Characterization of cell proliferation in the adult dentate under normal conditions and after kainate induced seizures using ribonucleotide reductase and BrdU. Brain Res. 1036, 7–17.